



## Ultimate strength of cylindrical shells with cutouts

Sang Eui Lee, Selcuk Sahin, Philippe Rigo, Minsue Park & Jeom Kee Paik

To cite this article: Sang Eui Lee, Selcuk Sahin, Philippe Rigo, Minsue Park & Jeom Kee Paik (2017) Ultimate strength of cylindrical shells with cutouts, *Ships and Offshore Structures*, 12:sup1, S153-S173

To link to this article: <http://dx.doi.org/10.1080/17445302.2016.1271592>



Published online: 21 Mar 2017.



Submit your article to this journal [↗](#)



View related articles [↗](#)



View Crossmark data [↗](#)

## Ultimate strength of cylindrical shells with cutouts

Sang Eui Lee<sup>a</sup>, Selcuk Sahin<sup>b,c</sup>, Philippe Rigo<sup>b</sup>, Minsue Park<sup>d</sup> and Jeom Kee Paik<sup>a,d,e</sup>

<sup>a</sup>The Korea Ship and Offshore Research Institute (The Lloyd's Register Foundation Research Centre of Excellence), Pusan National University, Busan, Republic of Korea; <sup>b</sup>Naval Architecture and Transport Systems Department (LHCN), University of Liège, Liège, Belgium; <sup>c</sup>Laboratoire d'Hydrodynamique, Énergétique et Environnement Atmosphérique (LHEEA), Ecole Centrale de Nantes, Nantes, France; <sup>d</sup>Department of Naval Architecture and Ocean Engineering, Pusan National University, Busan, Republic of Korea; <sup>e</sup>Department of Mechanical Engineering, University College London, London, UK

### ABSTRACT

Cutouts – perforations that are often made in wind turbine towers to allow access or passage – can also reduce the towers' ultimate strength. Thus, cutouts may need to be included in the ultimate strength formulations for wind turbine towers as an influential parameter, where significant. The aims of this study are to examine the effects of cutouts on the ultimate-strength characteristics of wind turbine towers and to propose empirical formulae to predict the reduced ultimate strength under axial compression and pure bending. The structural features of cutouts and towers in real wind turbines are investigated, and the effects of different design variables – such as shape, location, aspect ratio, column slenderness ratio, and column aspect ratio – on the ultimate-strength behaviour are described. The ultimate strengths of the towers are computed using elastic–plastic large-deflection finite element analyses. Empirical formulae accommodating a whole range of actual dimensional characteristics of cutouts and towers are derived and proposed. The findings of this research and the proposed formulae have the potential to enhance the structural design and safety assessment of wind turbine towers.

### ARTICLE HISTORY

Received 28 September 2016  
 Accepted 9 December 2016

### KEYWORDS

Cutouts; ultimate strength; wind turbine tower; parameters of influence; nonlinear finite element method

### Nomenclature

$A$	Area of the cutout	$T$	Torque moment
$b$	Breadth of the cutout	$u_x, u_y, u_z$	Translational restraints in the $x$ -, $y$ - and $z$ -axis
$b_f$	Breadth of the flange	$w_o$	Initial imperfection
$D_{in}, D_{out}$	Inner and outer diameter of the flange	$W$	Weight
$D(D_{max}/D_{min})$	Diameter (maximum/minimum) of the wind turbine tower	$\alpha$	Aspect ratio (height to breadth) of the cutout
$E$	Elastic modulus of the material	$\beta$	Slenderness ratio (breadth to thickness) of the cutout
$F_R$	Reference force of the wind turbine tower	$\delta_{max}$	Maximum deformation
$F_{Tower}$	Force acting on the wind turbine tower	$\gamma$	Column aspect ratio (height to diameter) of the wind turbine tower
$F_u$	Ultimate force of the wind turbine tower	$\gamma_{max}/\gamma_{min}$	Maximum/minimum column aspect ratio (height to maximum/minimum diameter) of the wind turbine tower
$F_{wind}$	Thrust induced by blades	$\lambda$	Column slenderness ratio (diameter to thickness) of the wind turbine tower
$F_z$	Load in $z$ -axis	$\lambda_{max}/\lambda_{min}$	Maximum/minimum column slenderness ratio (maximum/minimum diameter to maximum/minimum thickness) of the wind turbine tower
$h$	Height of the cutout	$\nu$	Poisson's ratio
$h_f$	Height of the flange	$\theta$	Angle of the cutout in the circumferential direction
$h_o$	Distance from the lower end to the centre of the cutout	$\theta_x, \theta_y, \theta_z$	Rotational restraint in the $x$ -, $y$ - and $z$ -axis
$H$	Height of the wind turbine tower	$\sigma$	Coefficient of correlation
$H_S$	Height of first section	$\sigma_Y$	Yield stress of the material
$M$	Pure bending moment	$\xi_D, \xi_t, \xi_h, \xi_b, \xi_C$	Coefficients of empirical formula for axial compression
$M_u$	Ultimate bending moment	$\zeta_D, \zeta_t, \zeta_h, \zeta_b, \zeta_C$	Coefficients of empirical formula for pure bending
$M_P$	Plastic bending moment		
$M_y$	Pure bending moment in $y$ -axis		
$r$	Radius		
$R$	Corner radius of the cutout		
$R^2$	Adjusted $R$ -square		
$t(t_{max}/t_{min})$	Thickness (maximum/minimum) of the wind turbine tower		
$t_c$	Thickness of the cutout		

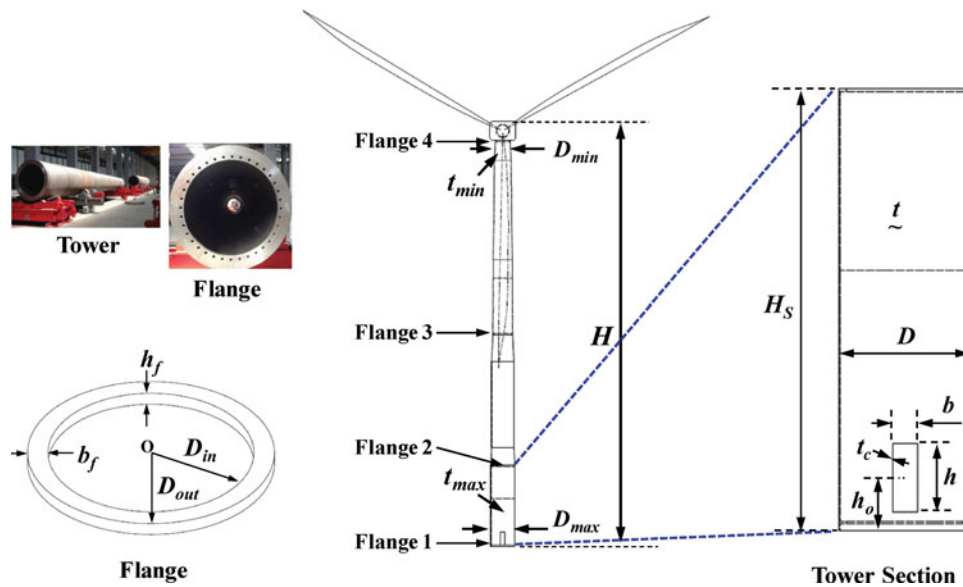


Figure 1. Schematic representation of a wind turbine tower. (This figure is available in colour online.)

## 1. Introduction

Cutouts are widely used in steel structures to provide access to or lighten the structure. It is no wonder, then, that these perforations reduce both the buckling and ultimate strength of such structures. In particular, wind turbines, which have relatively large doors, can be exposed to considerable strength reduction that could result in significant structural failure in their towers. It is thus of great importance to develop advanced technologies that can predict a tower's reduced strength using the size of the cutout.

The regulations for designing reliable and safe wind turbines have been developed and recommended by various authorities (ECCS 1980; DIN 18800-4 1990; EN1993-1.6 2006; DNVGL 2013a; DNVGL 2013b). However, there are no detailed guidelines for predicting the reduced strength of towers.

It is noted that there have been far fewer useful research attempts to investigate the effects of cutouts on the structural capacity of circular cylindrical shells than those investigating plates (Sabir & Chow 1983; Brown & Yettram 1986; Azizian & Roberts 1983; Shangmugam et al. 1999; Durban & Zuckerman 1999; Betten & Shin 2000; El-Sawy et al. 2004; Paik 2007; Kim et al. 2009; Wang et al. 2009). For a couple of decades, a number of studies were conducted to provide buckling analyses of circular cylindrical shells (Brazier 1927; Reissner 1961; Seide & Weingarten 1961; Fabian 1977; Gellin 1980) with cutouts under axial compression (Schenk & Schuëller 2007; Shariati & Rokhi 2010; Ghazijahani et al. 2015) and pure bending (Yeh et al. 1999; Dimopoulos & Gantes 2012, 2013, 2015; Guo et al. 2013; Dimopoulos et al. 2015).

The aims of this study are to use nonlinear finite element analysis to examine the effect of cutouts on the ultimate-strength characteristics and to propose simple formulae to estimate the reduced ultimate strength of wind turbine towers under axial compression and pure bending. The structural features of wind turbines are investigated using data collected from 102 wind turbines in service. Finite-element modelling techniques are developed to calculate the ultimate-strength

behaviour of the towers with a variety of design variables, such as cutout shapes and locations, aspect ratios, column slenderness ratios and column aspect ratios. The developed nonlinear finite element method modelling is then validated. For the parametric series analyses, a design of experiment (DOE) method, such as central composite design (CCD), is applied. Numerical computations are then used to derive a plausible empirical formula that predicts the ultimate strength of the towers.

## 2. Literature review

In the early days, buckling analyses of circular cylindrical shells subjected to pure bending and axial compression were first conducted by analytical and experimental manners. In particular, Brazier (1927) noted that the ultimate strength is directly related to the ovalisation of the tube cross-section under bending, and thus derived an expression for the strain energy per unit tube length in terms of the change in axial curvature. Reissner (1961) further developed a more general formulation for thin-walled cylindrical shells of arbitrary cross-sections. Seide and Weingarten (1961) used a modified Donnell equation and the Galerkin method and found that the maximum elastic buckling stress under bending is equal to the critical compressive stress under axial compression. Sherman (1976) experimentally identified that shells with a column slenderness ratio where  $\lambda$  was greater than about 50 did not have sufficient plastic hinge rotation capacity to develop the classical ultimate strength. Fabian (1977) observed two modes of failure of infinitely long cylindrical elastic shells subjected to bending, pressure and axial loads, and found that the circumferential flattening that constituted an ultimate load and compression wrinkles generated bifurcation buckling axially. Gellin (1980) demonstrated how extending the results of Brazier (1927) into the plastic range confirmed the results of limit states observed by Fabian (1977).

Traditionally, experimental tests have been regarded as the most efficient way of obtaining technical solutions, despite their

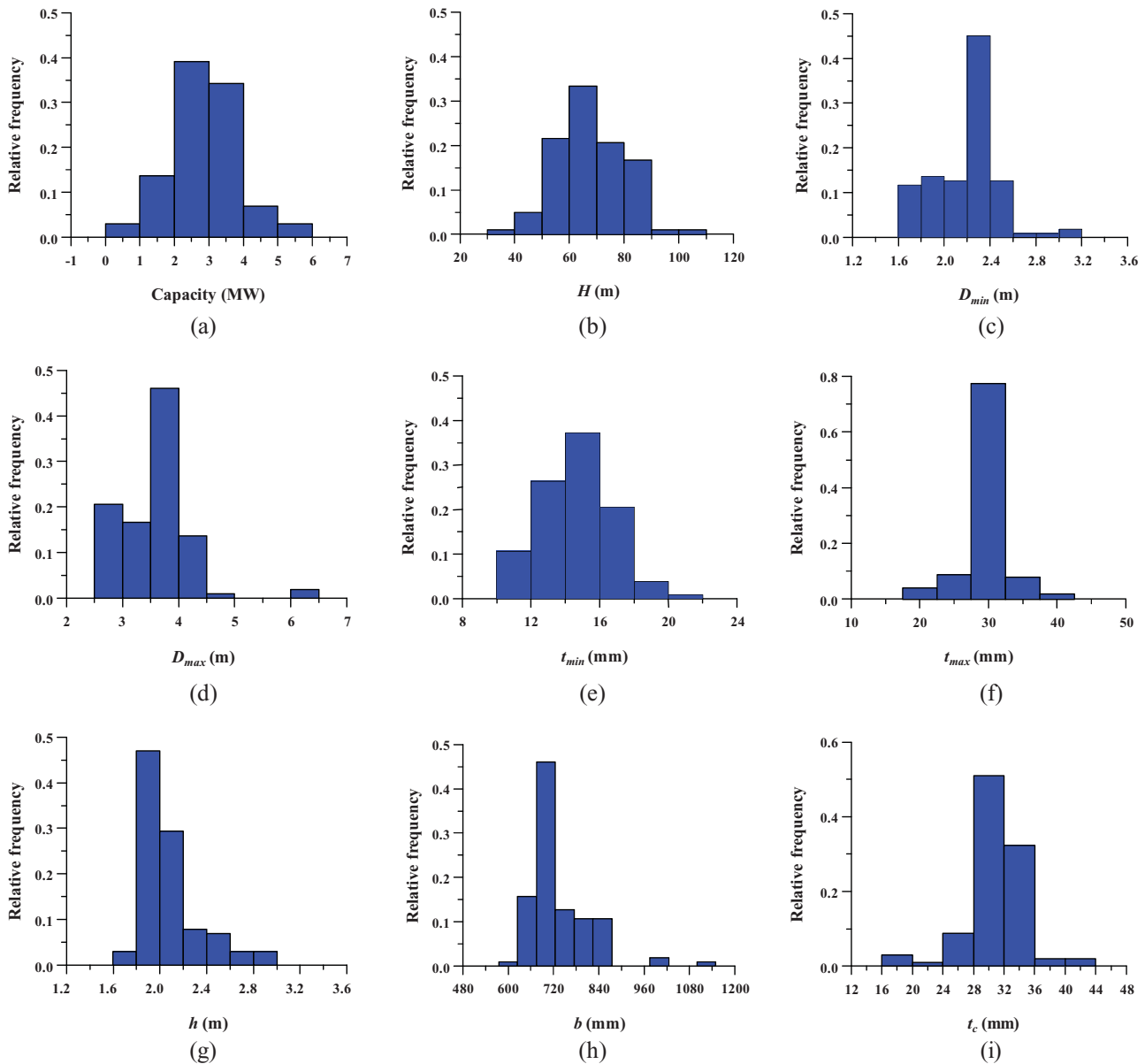


**Figure 2.** Characteristics of the wind turbine tower and the cutout: (a) capacity; (b) height; (c) min. diameter; (d) max. diameter; (e) min. thickness; (f) max. thickness; (g) height of the cutout; (h) width of the cutout; (i) thickness of the cutout. (This figure is available in colour online.)

high costs. Over the past 50 years, computing speeds and the capabilities of numerical tools have improved significantly. Hence, the contributions made by numerical simulations to engineering applications are increasing. The same trend has been observed in the wind turbine industries, and extensive experimental tests and numerical simulations have been conducted to examine the load-carrying capacity of circular cylindrical shells with cutouts under axial compression and pure bending.

For axial compression, Tennyson (1968) experimentally observed membrane stress distributions and isoclinic patterns around the edges of cutouts using photoelastic shells. Jullien and Limam (1998) found that the buckling strength is sensitive to a cutout's angle or circumferential size, based on parametric studies of its shape (square, rectangular, circular) and dimensions (axial and circumferential sizes, diameter).

Furthermore, they pointed out the importance of initial imperfections for numerical simulations. Schenk and Schuëller (2007) studied the effects of random geometric imperfections on the critical load of thin-walled cylindrical shells under axial compression with rectangular cutouts. They found that the coefficient of variation of the critical load did not decrease with the imperfections' magnitude. Han et al. (2006) observed that the location and size of a cutout significantly affect the buckling load; specifically, cutouts located near the fixed boundary could effectively absorb energy and redistribute the load more efficiently. Shariati and Rokhi (2008, 2010) reported that longer shells exhibit much more sensitivity to the positions of the cutouts. Moreover, they observed that the buckling strength decreases as height increases with a constant cutout width. Ghanbari Ghazijahani et al. (2015) experimentally found a symmetric ring-shaped bulging wave in an intact specimen

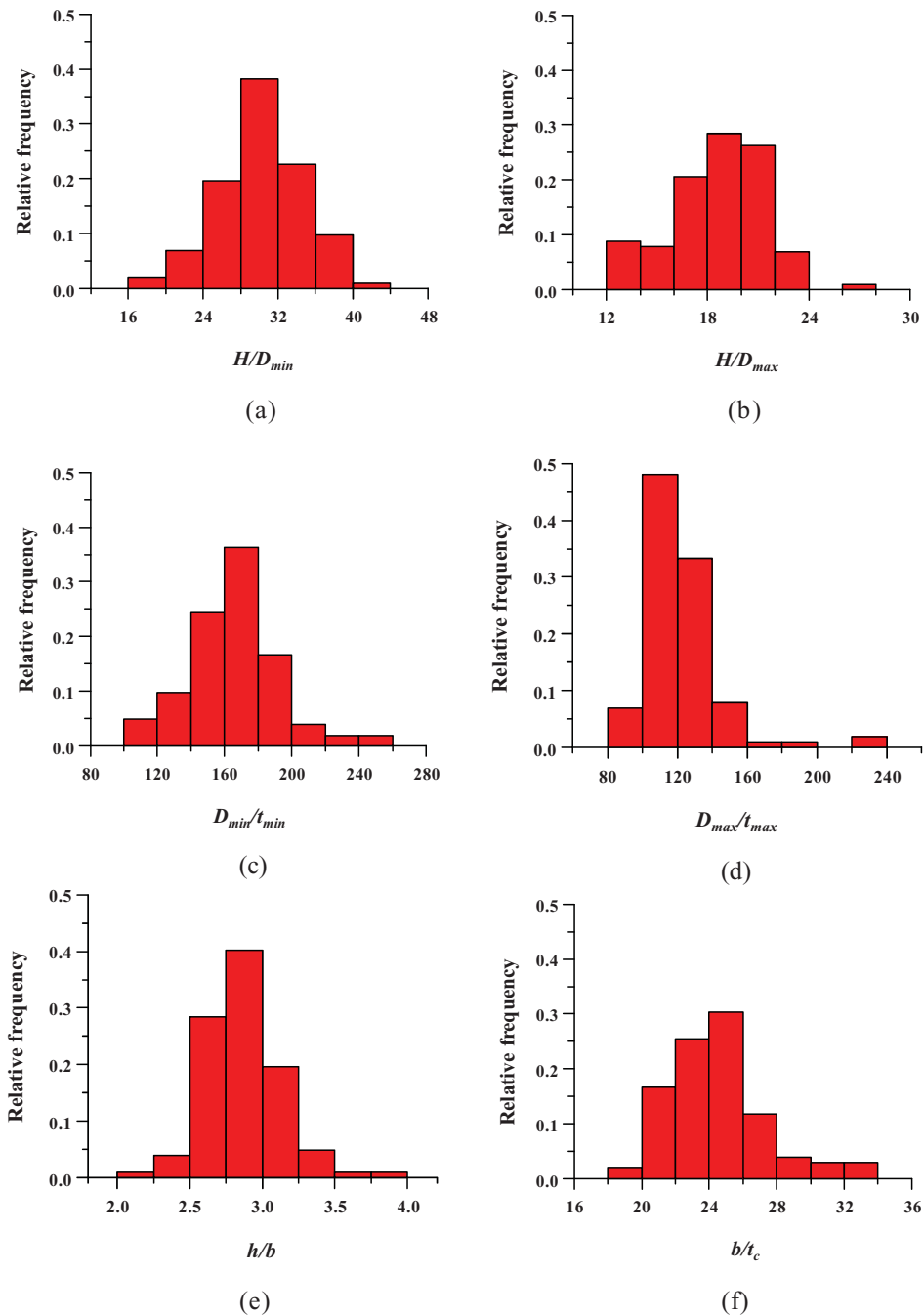


**Figure 3.** Geometrical characteristics: (a) height to min. diameter ratio; (b) height to max. diameter ratio; (c) min. diameter to min. thickness ratio; (d) max. diameter to the max. thickness ratio; (e) height to width ratio of the cutout; (f) width to thickness ratio of the cutout. (This figure is available in colour online.)

**Table 1.** Actual range and the most probable dimensions of the wind turbine and the cutout.

Parameter	Range	Most probable	Parameter	Range	Most probable
Capacity (MW)	0.5–5.0	2.5	$t_{max}$ (mm)	16–40	30
$H$ (mm)	37,000–100,000	65,000	$\gamma_{min}$	17.5–42.1	30.0
$h$ (mm)	1640–2900	1900	$\gamma_{max}$	12.0–27.7	19.0
$b$ (mm)	620–1100	700	$\lambda_{min}$	100.0–250.0	170.0
$t_c$ (mm)	16–40	30.0	$\lambda_{max}$	95.7–222.2	110.0
$D_{min}$ (mm)	1600–3000	2300	$\alpha$	2.2–3.8	2.875
$D_{max}$ (mm)	2610–6000	3750	$\beta$	19.1–43.8	25.0
$t_{min}$ (mm)	10–20	15			

**Table 2.** Dimensions of the flanges.

No.	$D_{in}$ (mm)	$D_{out}$ (mm)	$b_f$ (mm)	$h_f$ (mm)
Flange1	3,350	3,750	200	70
Flange2	3,370	3,750	190	95
Flange3	2,760	3,150	170	88
Flange4	2,040	2,350	130	250

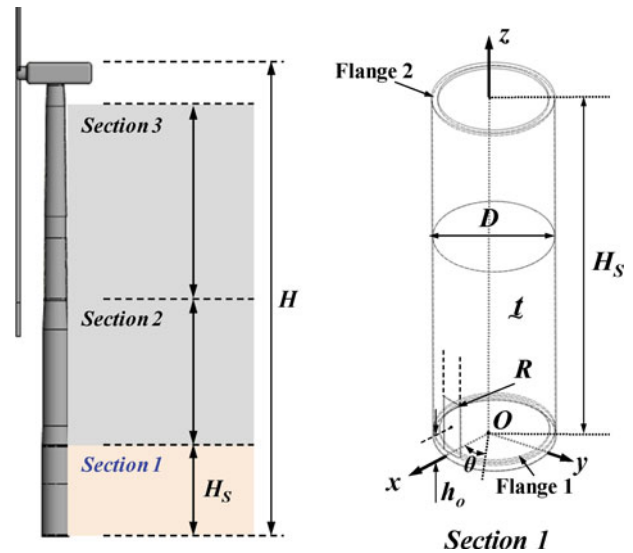
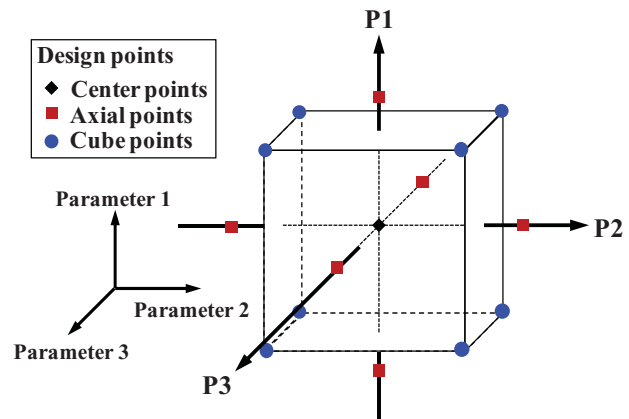
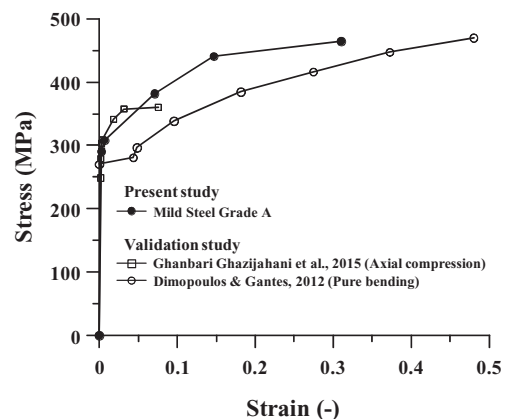
**Table 3.** Applied dimensions of cutout's shape.

Shape	$A(\times 10^6 \text{ mm}^2)$	$h$ (mm)	$b$ (mm)	$R$ (mm)
Rectangular	1.321	1900	700.0	100
Elliptical	1.321	1900	885.5	–
Half-rectangular–elliptical	1.321	1900	781.6	100

after initiating buckling. They noted that the effects of the cutouts' heights on the capacity were less than 5% under axial compression.

For pure bending, Kyriakides and Ju (1992) and Ju and Kyriakides (1992) observed that thinner shells developed short wavelength periodic ripples on the compressed sides of the shells, and the shells buckled locally and collapsed soon after the ripples appeared. In contrast, thicker shells were found to exhibit limited load instability as a direct consequence of the ovalisation of the shell cross-section caused by pure bending. Yeh et al. (1999) observed that for a shell with a circular cutout, the ultimate strength decreased as the diameter of the cutout increased, whereas for a shell with a rectangular cutout, the ultimate strength decreased as the size of the cutout increased. It was also found that the ultimate strength of a shell with a cutout on the compression side was less than for a cutout on the tension side, and the ultimate strength increased when a cutout was close to the end of the clamped shell. Guo et al. (2013) found that an increase in the  $D/t$  ratio resulted in a more pronounced local buckling phenomenon, with the stiffeners increasing the load-carrying capacity while improving the ductility.

The most distinguished numerical and experimental works were Dimopoulos's series of studies (Dimopoulos & Gantes 2012, 2013, 2015; Dimopoulos et al. 2015) on circular cylindrical shell structures. Experimental and numerical studies of the buckling behaviour of cantilevered circular cylindrical shells with cutouts and stiffening were conducted, and it was confirmed that the presence of the cutouts led to a reduction in strength. The lowest collapse load appeared when a cutout was situated on the compression side (Dimopoulos & Gantes 2012). It was also shown that simple stiffening types, consisting of either a peripheral frame or two longitudinal stiffeners with a ring, were particularly efficient and could be used instead of more complex examples (Dimopoulos & Gantes 2013). The importance of geometrical and material nonlinearities, including initial imperfections, was also noted (Dimopoulos & Gantes 2015). Finally, the stiffening effects of cutouts on circular cylindrical shells under dynamic wind loading were assessed using aeroelastic code. It was concluded that the dynamic effect led to a small decrease in tower strength compared to the effect obtained via static analysis, but this reduction was less than 10% in all investigated cases (Dimopoulos et al. 2015).

**Figure 4.** Schematic representation of applied geometries. (This figure is available in colour online.)**Figure 5.** Example of design points in CCD for three parameters (Lee et al. 2014). (This figure is available in colour online.)**Figure 6.** Stress–strain curves for the applied materials.

### 3. Structural features

#### 3.1. Definition of geometrical parameters

Wind turbines typically consist of circular cylindrical shell sections connected by bolted flanges, as shown in Figure 1. The geometrical attributes of a typical wind turbine tower



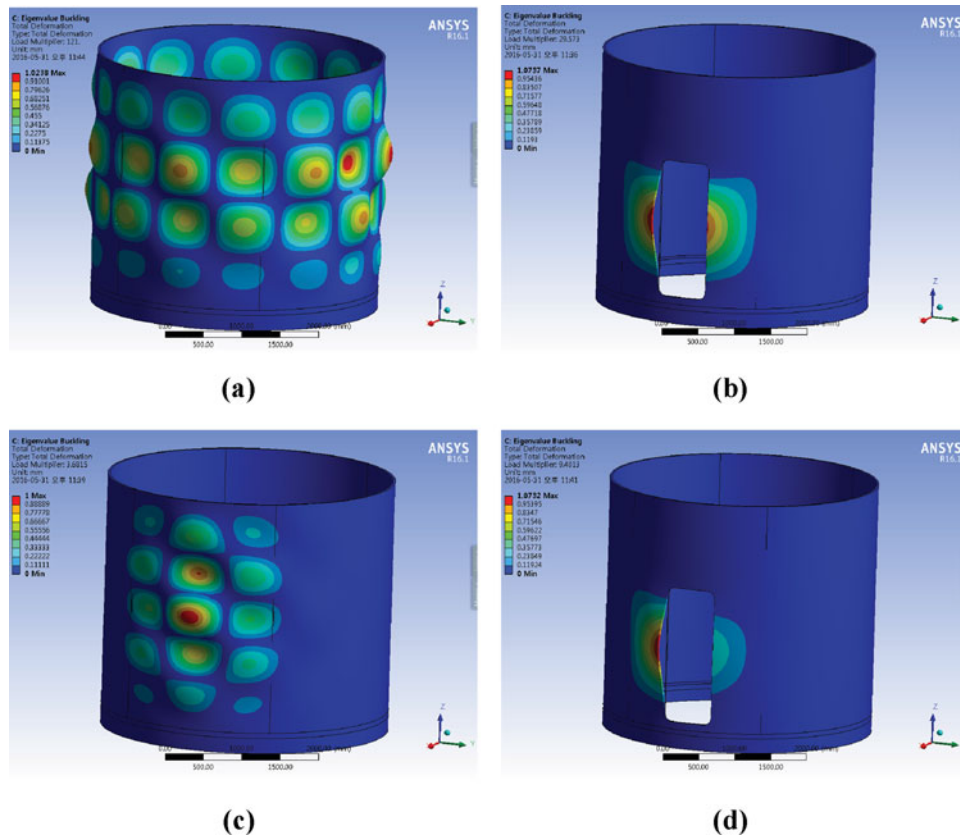


**Figure 7.** An example of first buckling mode: (a) intact under axial compression; (b) with the cutout under axial compression; (c) intact under pure bending; (d) with the cutout under pure bending. (This figure is available in colour online.)

with a cutout are defined here. The following four parameters for wind turbine towers are considered: minimum column aspect ratio ( $\gamma_{\min} = H/D_{\min}$ ); maximum column aspect ratio ( $\gamma_{\max} = H/D_{\max}$ ); minimum column slenderness ratio ( $\lambda_{\min} = D_{\min}/t_{\min}$ ) and maximum column slenderness ratio ( $\lambda_{\max} = D_{\max}/t_{\max}$ ). The other two cutout parameters considered are the aspect ratio ( $\alpha = h/b$ ) and the slenderness ratio ( $\beta = b/t_c$ ).

### 3.2. Geometrical features

Data on 102 wind turbines and their cutouts were collected where the capacities ranged from 0.5 to 5.0 MW. The principal features are displayed in Appendix (Tables A1 to A3), and the geometrical characteristics of each parameter predefined in Section 3.1 are analysed. The statistical distribution of the parameters is shown in Figures 2 and 3. Table 1 summarises the range and most probable values of each parameter. These findings are then used to identify the geometrical parameters of the standard wind turbine tower and the cutout:  $H = 65,000$  mm;  $D_{\max} = 3750$  mm;  $t_{\max} = 30$  mm;  $h = 1900$  mm;  $b = 700$  mm and  $t_c = 30$  mm ( $\alpha = 2.875$ ,  $\beta = 25.0$ ). Based on those parameters, the dimensions of the flanges are designed and illustrated in Table 2 (Sahin 2016). It was assumed that the standard wind turbine tower is composed of three sections, as shown in Figure 4, and that the height of the first section used in the present study was  $H_S = 12,655$  mm. Hereafter, because the tower section applied in the present study had a uniform thickness,  $t$ , the thickness of

the cutout ( $t_c$ ) and the maximum thickness of the wind turbine tower ( $t_{\max}$ ) are represented as the thickness of the wind turbine tower -  $t$  ( $= t_c = t_{\max}$ ) - and the diameter of the tower section ( $D$ ) is the same as the maximum diameter of the wind tower ( $D_{\max}$ ).

### 3.3. Selection of parameters

CCD is an experimental design for building a second-order model without needing to use a complete three-level factorial experiment. The CCD with the fractional factorial design was used in this study as a deterministic method for parameter selection. The locations of the design points were determined based on the number of input parameters, in accordance with the DOE method. The example points of the CCD with three input parameters are shown in Figure 5.

### 3.4. Reference capacity of circular cylindrical shells without the cutout

In the section on wind turbine structures with cutouts, the first yield occurred near the cutout where the highest compression developed and rapidly expanded around the cutout with further loading. The entire load-carrying capacity of the wind turbine structure with the cutouts depended on the geometrical dimensions and material properties. In the present study, the reference buckling loads of the shells without cutouts subjected to axial compression (Shariati & Rokhi 2008) and pure bending moments (Dimopoulos & Gantes 2013) were defined as

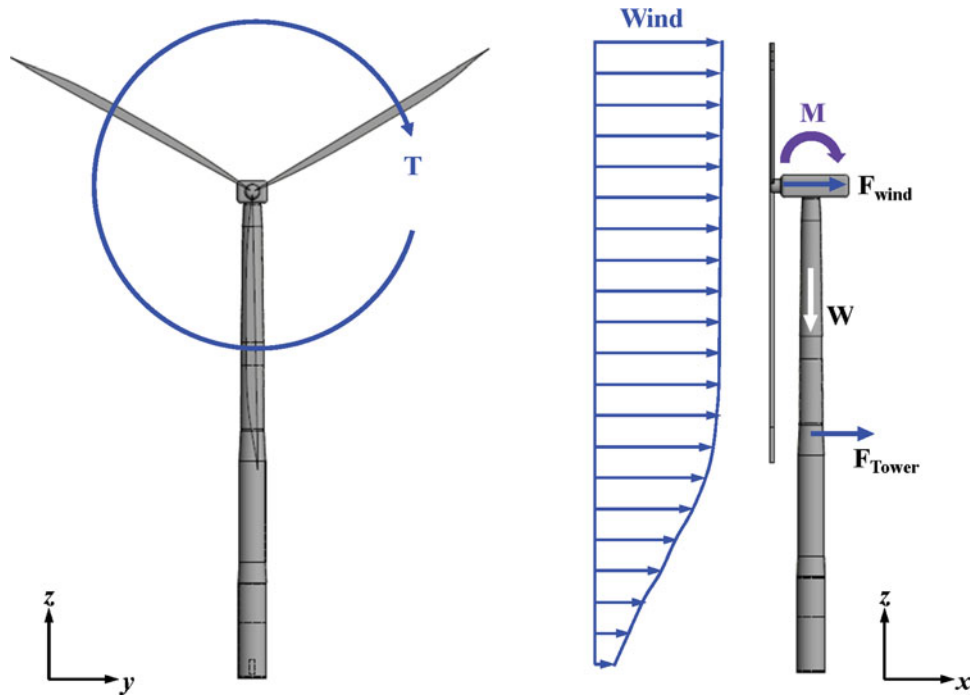


Figure 8. Schematic free-body diagram. (This figure is available in colour online.)

$$F_R = \pi D t \times \sigma_Y \quad (1)$$

$$M_P = \frac{4}{3} \sigma_Y \left( \left( r + \frac{t}{2} \right)^3 - \left( r - \frac{t}{2} \right)^3 \right) \quad (2)$$

where  $F_R$  is the reference load of a wind turbine,  $M_P$  is the plastic bending moment of a wind turbine,  $D$  is the diameter of the wind turbine tower,  $r$  is the radius of the wind turbine tower,  $t$  is the thickness of the wind turbine tower and  $\sigma_Y$  is the yield stress of the material.

## 4. Nonlinear finite-element modelling

### 4.1. Finite-element model

In this study, nonlinear finite element analysis is performed using ANSYS-Workbench (2015) to accommodate both geometrical and material nonlinearities. To solve highly nonlinear problems, including the very unstable snap-through response of shell structures, nonlinear stabilisation – which uses the line search method together with auto time stepping – is used.

The SHELL181 element, which has four nodes with 6 degrees of freedom at each node, is used to model circular cylinder shells and the SOLID185 element, which has eight nodes

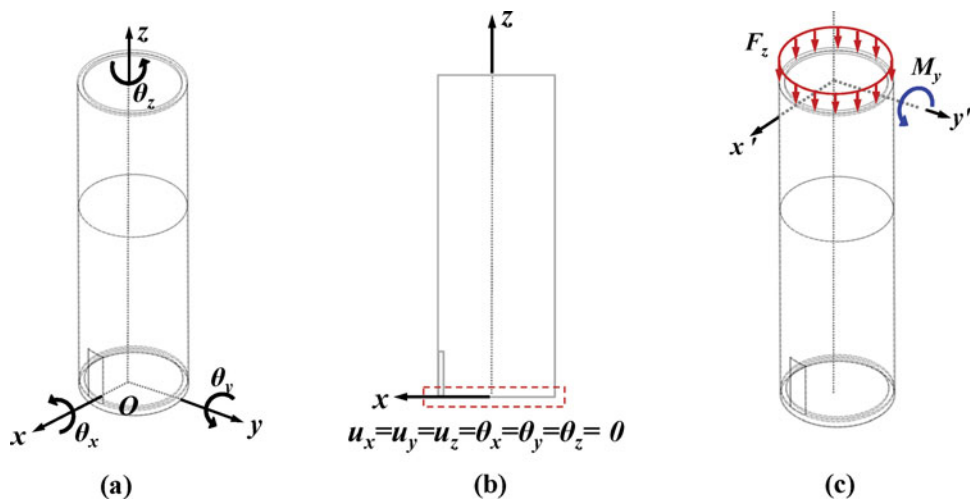


Figure 9. Coordinate system and applied boundary conditions of the wind turbine tower: (a) coordinate system; (b) fixed boundary condition; (c) applied loading conditions. (This figure is available in colour online.)



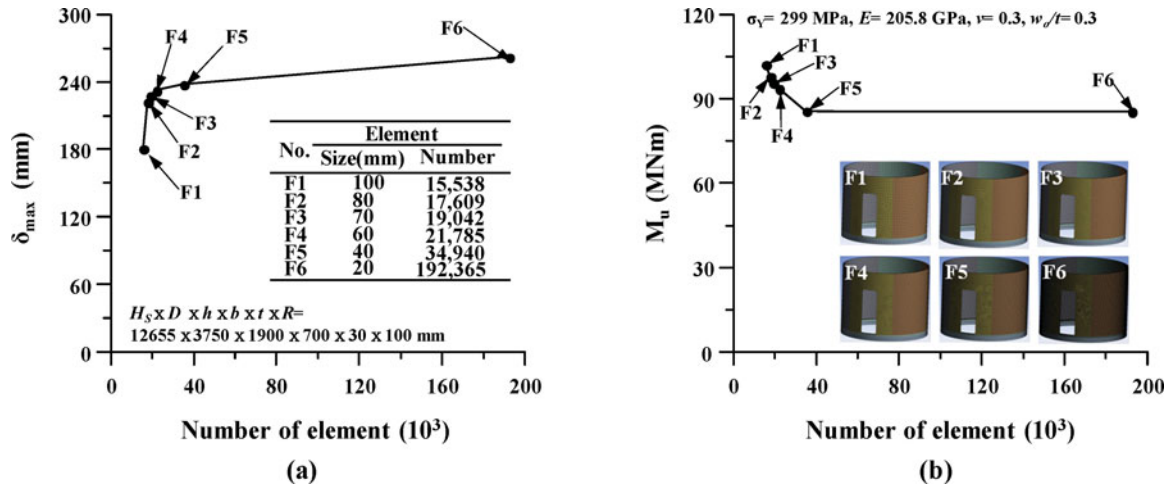


Figure 10. The result of mesh-convergence: (a) maximum deformation; (b) maximum bending moment. (This figure is available in colour online.)

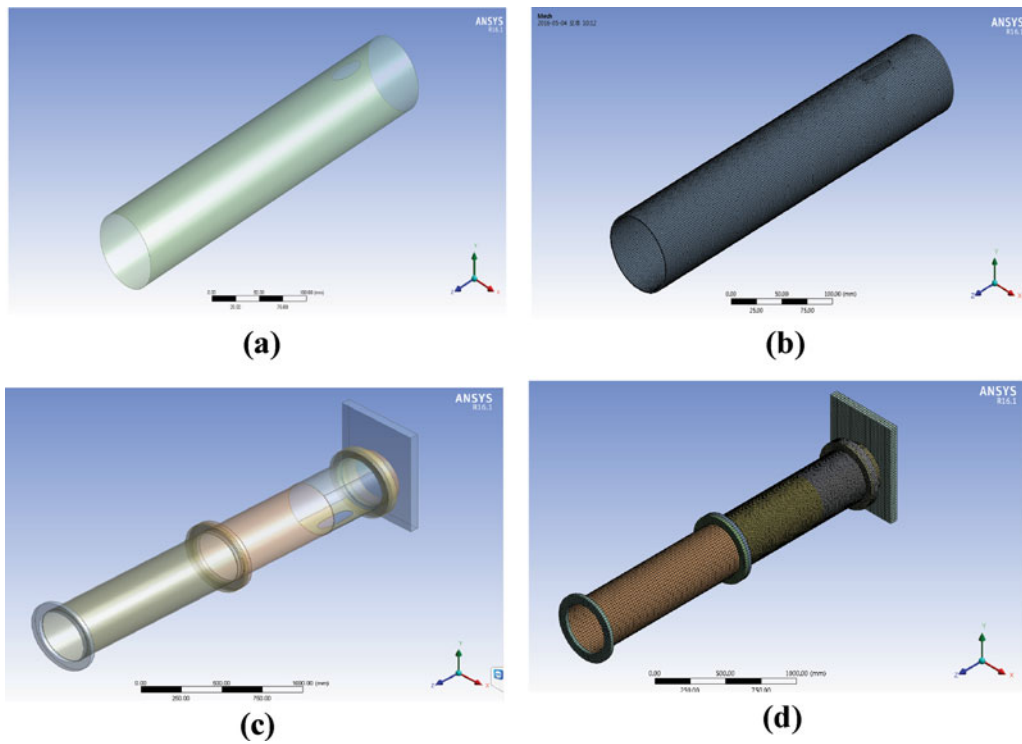


Figure 11. Geometries and mesh models of validation studies: (a) geometry for axial compression; (b) applied mesh for axial compression; (c) geometry for pure bending; (d) applied mesh for pure bending. (This figure is available in colour online.)

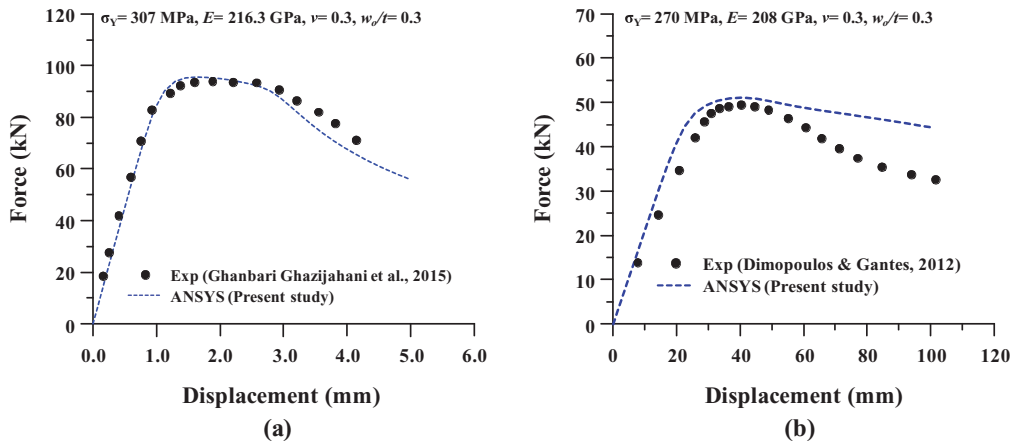
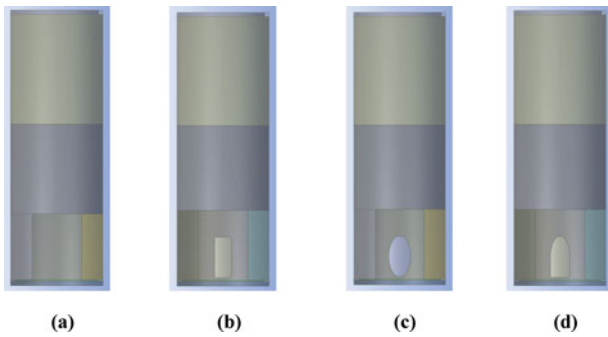


Figure 12. Collapse mechanism of the wind turbine tower: (a) axial compression; (b) pure bending. (This figure is available in colour online.)



**Figure 13.** An example of applied geometries: (a) intact (no-opening); (b) rectangular; (c) elliptical; (d) half-rectangular–elliptical. (This figure is available in colour online.)

with 3 degrees of freedom at each node, is used to model the ring frame located at both ends of the circular cylinder shell section. The wind turbine is modelled on the result of the quasi-static material test of mild steel grade A, as shown in Figure 6.

As in previous studies (Jullien & Limam 1998; Schenk & Schuëller 2007; Dimopoulos & Gantes 2015), the effect of initial imperfection is properly applied. The maximum magnitude of initial deflection  $w_o$  is assumed to be 30% of the thickness of the wind turbine tower; that is,  $w_o = 0.3t$ . The eigenvalue buckling mode is used to determine the shape of the initial deflection. Figure 7 provides examples of the smallest buckling mode near the cutout, obtained from the eigenvalue buckling analyses for intact (no-opening) and cutout under axial compression and pure bending. In order to maintain the simplicity of finite element method computations, the residual stress caused by welding is not considered in the present study.

#### 4.2. Loading conditions

The loading regimes of wind turbines during operation are extremely complex. A proper understanding of loads on wind turbines and their structural responses are crucial to avoiding their catastrophic failure. In general, the types of loads acting

on wind turbines in service can be classified into five categories: static, cyclic, stochastic, aerodynamic and mechanical. As shown in Figure 8, the schematic free-body diagram of a wind turbine structure can be represented as three loads: a torque due to the blades, an axial force due to gravity and a bending moment due to the thrust of the blades and the transverse force on a tower.

In the present study, it is assumed that an axial force and bending moment are closely related to the wind turbine tower's failure or collapse. They are applied in an isolated manner rather than in combination to investigate the effect of each load on the ultimate strength of the wind turbine tower with a cutout. When it is essential to predict the ultimate strength accurately, the combined loads and the shear force should be properly considered.

#### 4.3. Boundary conditions

The boundary conditions investigated in this study are described in Figure 9. The coordinate system used for their measurement is shown in Figure 9(a). The restraints are described in detail as following:

- Fixed boundary condition, as shown in Figure 9(b)
- Bottom surface: translational restraints in the  $x$ -,  $y$ - and  $z$ -directions,  $u_x = u_y = u_z = 0$ ; rotational restraint in the  $x$ -,  $y$ - and  $z$ -directions,  $\theta_x = \theta_y = \theta_z = 0$ .

As mentioned, a wind turbine with a cutout – as detailed in Section 3.2 – is regarded as being subject to axial compression in the  $z$ -axis and pure bending in the  $y$ -axis, as shown in Figure 9(c).

#### 4.4. Mesh-convergence study

This section presents the results of the mesh-convergence study for six types of element sizes under pure bending when  $\sigma_Y = 299$  MPa and  $w_o = 0.3t$ . In the mesh-convergence study, six element sizes are tested under pure bending. The ultimate strength is summarised in Figure 10, and it is found that approximately 35,000 elements (F5, size = 40 mm) are sufficient to estimate the ultimate bending moment of the wind turbine. The authors

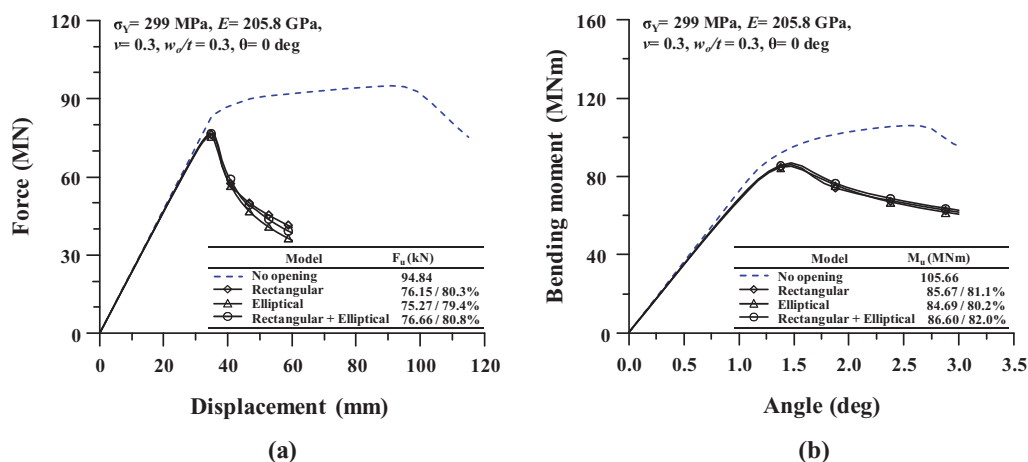


**Figure 14.** Effects of cutout shapes on load-carrying capacity: (a) axial compression; (b) pure bending. (This figure is available in colour online.)

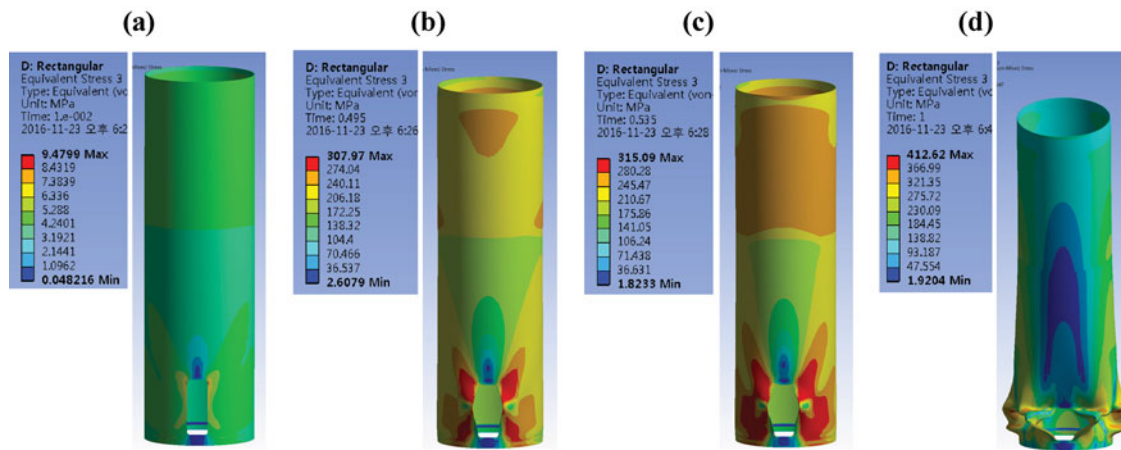
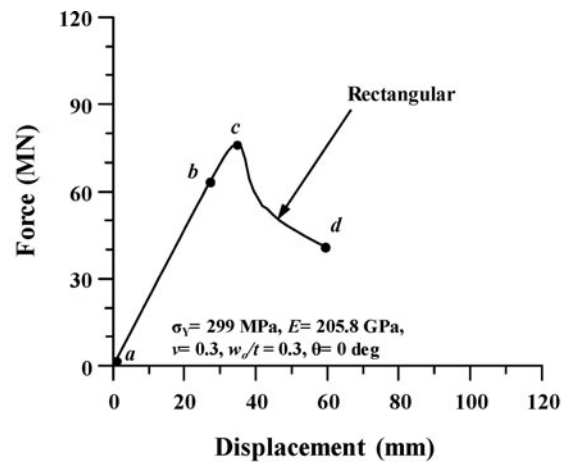


**Figure 15.** von Mises stress distribution at various loading stages under axial compression for standard wind turbine model with the rectangular cutout (scale factor = 10). (This figure is available in colour online.)

assume that the mesh-convergence for axial compression may agree with the results for pure bending.

#### 4.5. Validation

The finite-element modelling techniques developed in the present study are validated by the experimental results under axial compression (Ghanbari Ghazijahani et al. 2015) and pure bending (Dimopoulos & Gantes 2012). Figure 11 shows the results of a validation study for the models shown in Figure 12. It confirms that the developed finite-element modelling technique is generally effective for simulating the ultimate strength of the wind turbine towers under axial compression and pure bending.

### 5. Effects of variables

In this section, three sets of parametric studies of the results are presented. First, to investigate the effect of a cutout shape on the ultimate strength, three shapes – rectangular, elliptical and half-elliptical–rectangular – are considered. Second, to examine the effect that a cutout location has on the ultimate strength in the vertical and circumferential directions, five locations in the vertical direction and nine in the circumferential direction are considered. Third, the cutout shape, aspect ratio, column slenderness (diameter to thickness) ratio and column aspect

(height to diameter) ratio are taken as the design variables and their effects on the ultimate strength are widely calculated. To identify the combined effects of these variables on the ultimate strength, a DOE with the CCD method is applied for the selection of design points for a given range of each parameter from Section 3.2.

#### 5.1. Effects of cutout shape

As stated earlier, previous researchers (Julien & Limam 1998; Yeh et al. 1999) attempted to examine the effects of cutout shape on the load-carrying capacities of circular cylindrical shells. They concluded that the existence of cutouts alters the nature of the moment-end-rotation response under pure bending. However, the effects of cutout shape on the load-carrying capacities were weak, and sometimes negligible.

The authors attempted to improve their understanding of the effects of cutout shape on the ultimate strength using the standard model predefined in Section 3.2. Three types of shapes – rectangular, elliptical and half-rectangular–elliptical – were considered. To perform an accurate comparison, the area of each cutout,  $A$ , was kept the same. The parameters considered in this study are as follows:

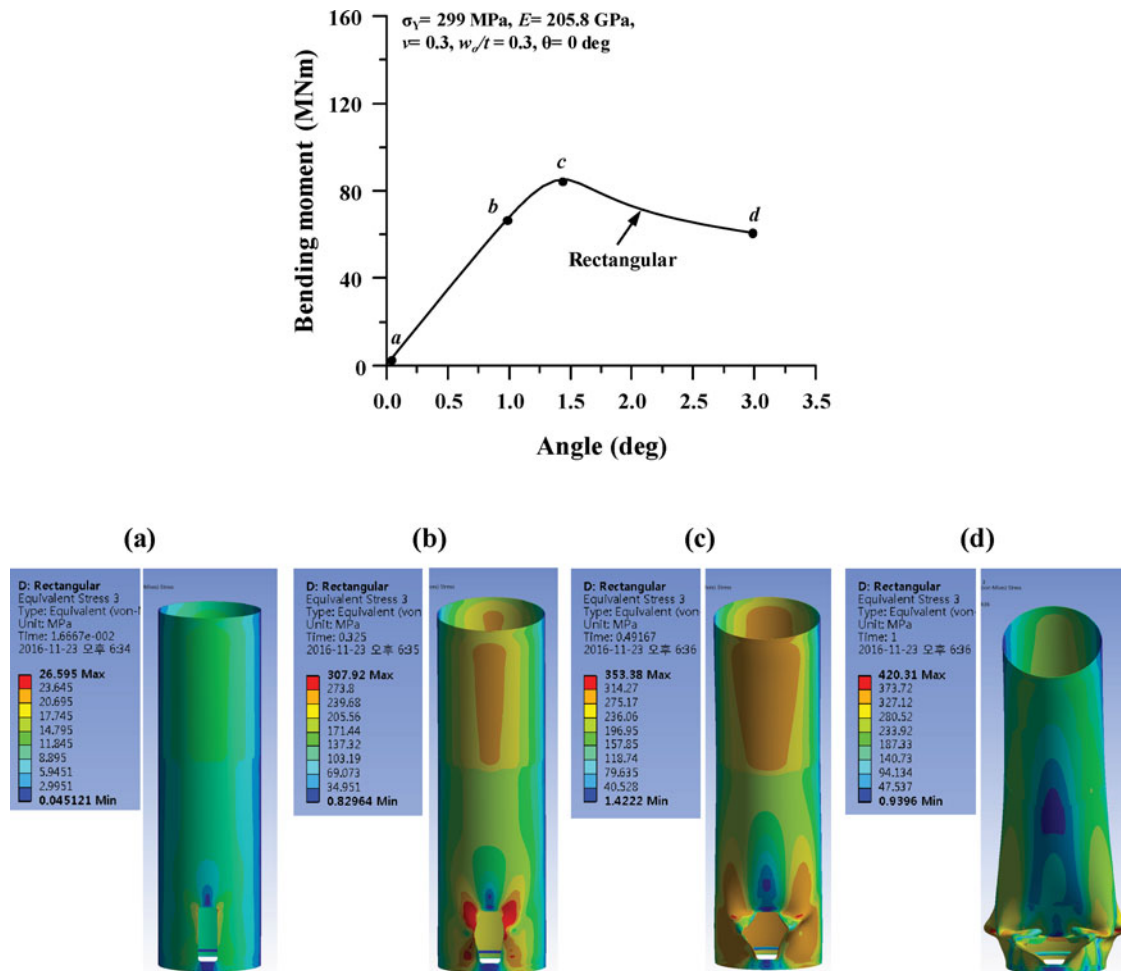


Figure 16. von Mises stress distribution at various loading stages under pure bending for standard wind turbine model with the rectangular cutout (scale factor = 10). (This figure is available in colour online.)

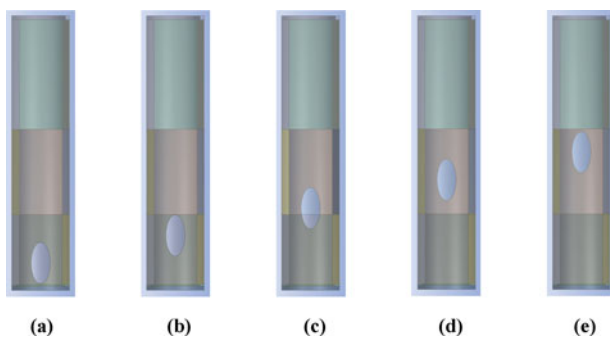


Figure 17. An example of applied geometries with varying cutout location in vertical direction: (a)  $h_o/H_s = 0.1$ ; (b)  $h_o/H_s = 0.2$ ; (c)  $h_o/H_s = 0.3$ ; (d)  $h_o/H_s = 0.4$ ; (e)  $h_o/H_s = 0.5$ . (This figure is available in colour online.)

- Shape: intact (no-opening), rectangular, elliptical, half-rectangular-elliptical
- Loading condition: axial compression, pure bending

The applied geometries are illustrated in Figure 13, and their dimensions for the cutouts are summarised in Table 3. Figure 14 describes a comparison of the load-carrying capacity with the

no-opening model. The reduction rate of the ultimate strength of each shape for both loading conditions appeared to be around 80% intact. The present results confirm the previous findings (Julien & Limam 1998; Yeh et al. 1999) that the effect of shape is negligible.

Figures 15 and 16 illustrate von Mises stress contours at various loading stages for the standard wind turbines with the rectangular cutout under axial compression and pure bending as an example. It was found that the stress concentration is initiated regions around the cutout and it increases with the further load. As it increases, the level of stress rapidly rises so that these regions yield before the tower reaches the buckling state. Finally, tower shell around the cutout buckles. It was surmised that the local buckling occurs at first around the cutout and then the tower buckling follows.

## 5.2. Effects of cutout location

The effects of cutout location in the vertical or circumferential directions were previously investigated by a number of researchers (Ju & Kyriakides 1992; Kyriakides & Ju 1992; Yeh et al. 1999; Han et al. 2006; Dimopoulos & Gantes 2012), who noted that as the cutout location neared the boundaries, the

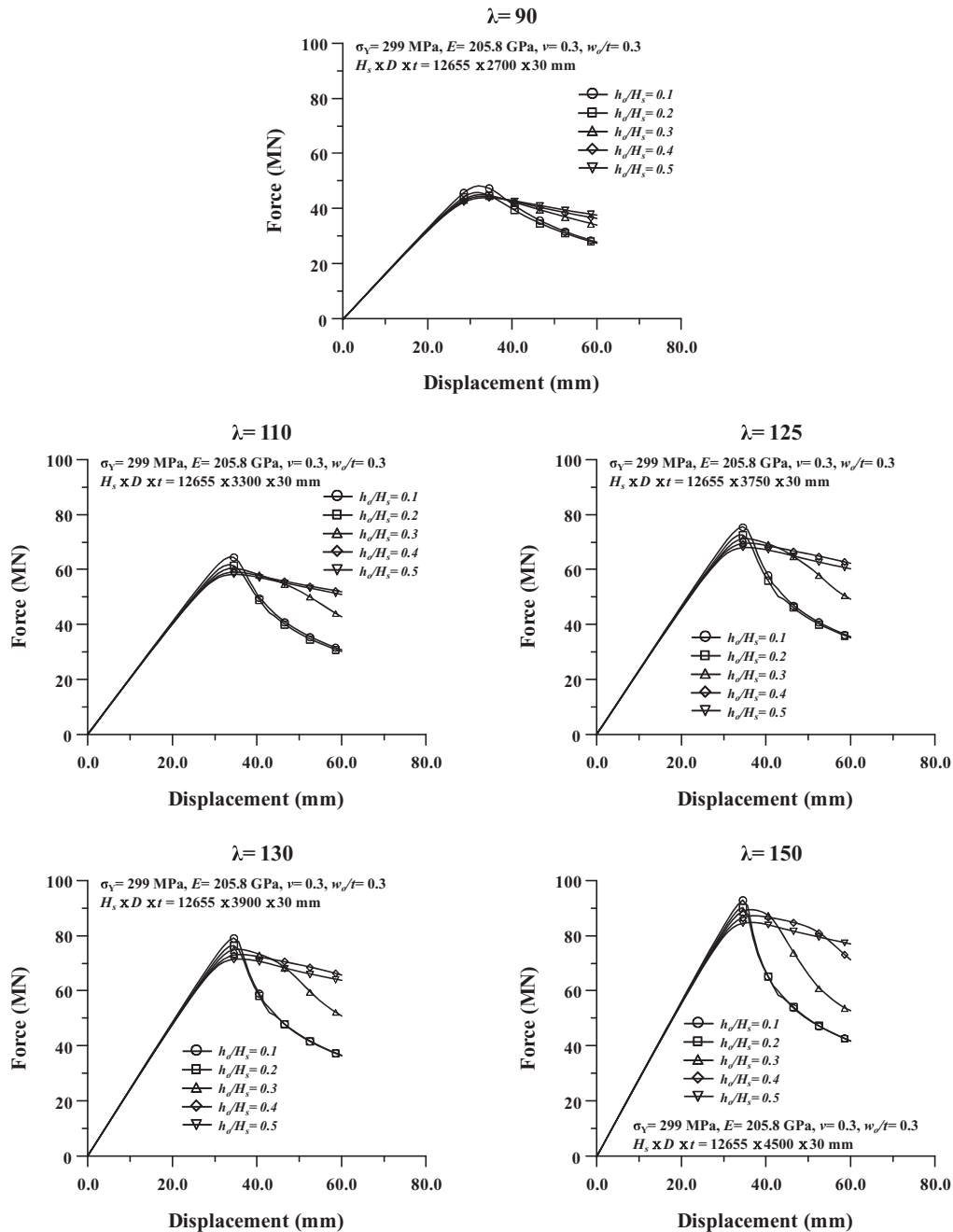


Figure 18. Effects of cutout locations under axial compression.

ultimate strength increased under axial compression. Moreover, the ultimate strength of a circular cylindrical shell with a cutout on the compression side was smaller than that of one with a cutout on the tension side under pure bending (Ju & Kyriakides 1992; Kyriakides & Ju 1992; Yeh et al. 1999; Dimopoulos & Gantes 2012). In order to assess the ultimate strength of circular cylindrical shells with cutouts, a series of nonlinear finite element method computations are performed for various cutout locations in the vertical and circumferential directions.

### 5.2.1. Vertical direction

To investigate the effects of cutout location in the vertical direction on the ultimate strength, the thickness,  $t$ , is kept the same

at 30 mm. Fifty cases of series analyses were performed, and the parameters considered are as follows:

- Shape: elliptical
- Location in vertical direction,  $h_o/H_s$ : 0.1, 0.2, 0.3, 0.4, 0.5
- Column slenderness ratio,  $\lambda = D/t$ : 90, 110, 125, 130, 150
- Loading condition: axial compression, pure bending

Figure 17 displays an example of applied geometries with varying cutout locations in the vertical direction,  $h_o/H_s = 0.1-0.5$ .

Figures 18 and 19 illustrate the force-displacement and moment-rotation histories for various column slenderness

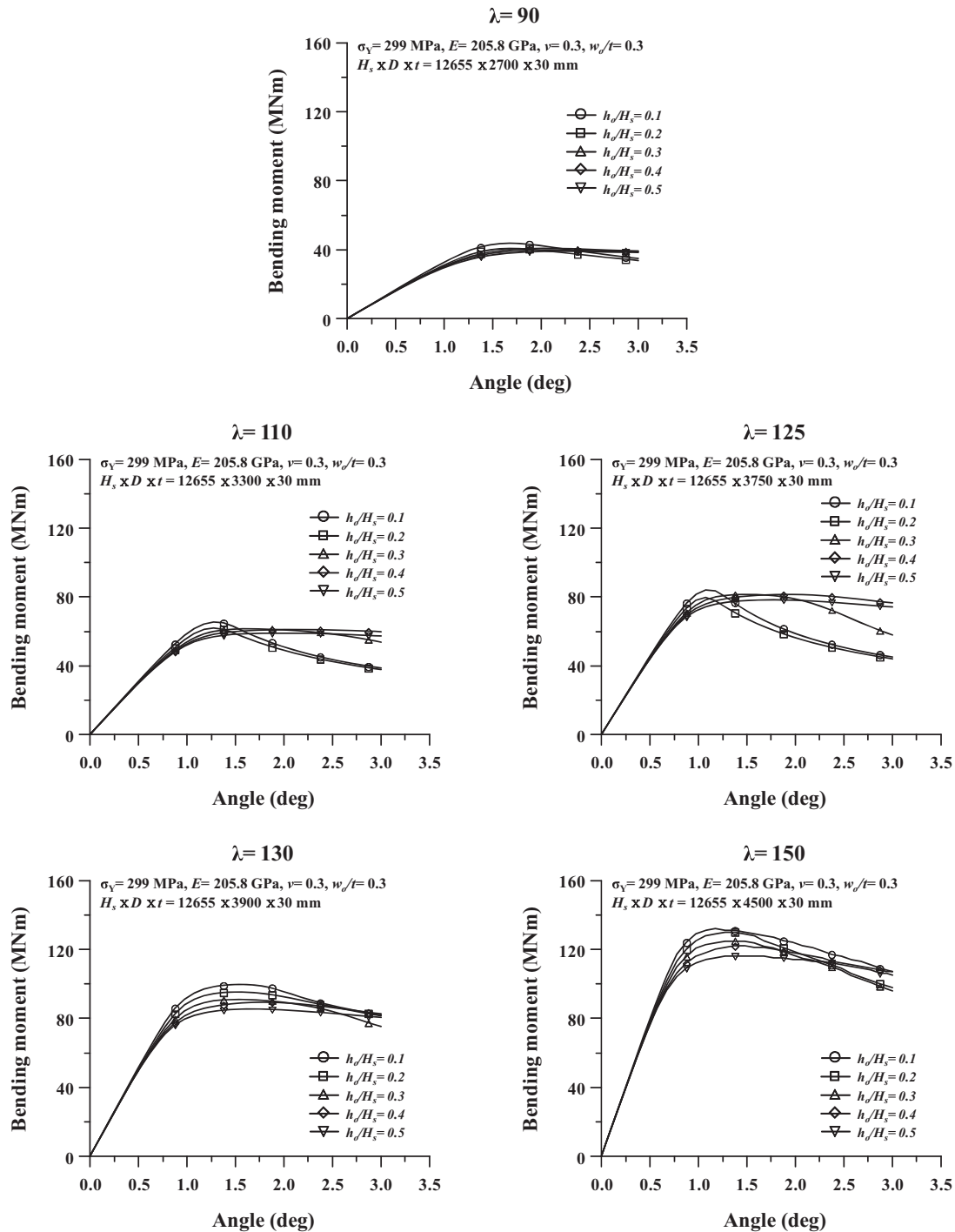


Figure 19. Effects of cutout locations under pure bending.

ratios. It was found that the closer the cutout is to the fixed boundary, the more the ultimate strength increases in both loading conditions. However, while numerical results of cutouts located near the fixed boundaries measured the higher ultimate strength than others, a sudden drop in strength appears after the ultimate state for all cases in axial compression and some cases in pure bending. Although the closest cutout reveals the highest ultimate strength, it cannot be regarded as the safest wind turbine in terms of structural integrity. It indicates that current locations of the cutout in the vertical axis may

not be the optimum location in terms of safety and structural integrity. Therefore, it is recommended that when structural engineers determine the location of the cutout in the vertical direction, they must carefully consider it as one of crucial design aspects and have a design solution for enhancing structural capacity.

Figure 20 summarises the non-dimensionalised load-carrying capacity, which varies with the cutout location in the vertical direction. The ultimate strength increases almost linearly as a function of the cutout location, and as the



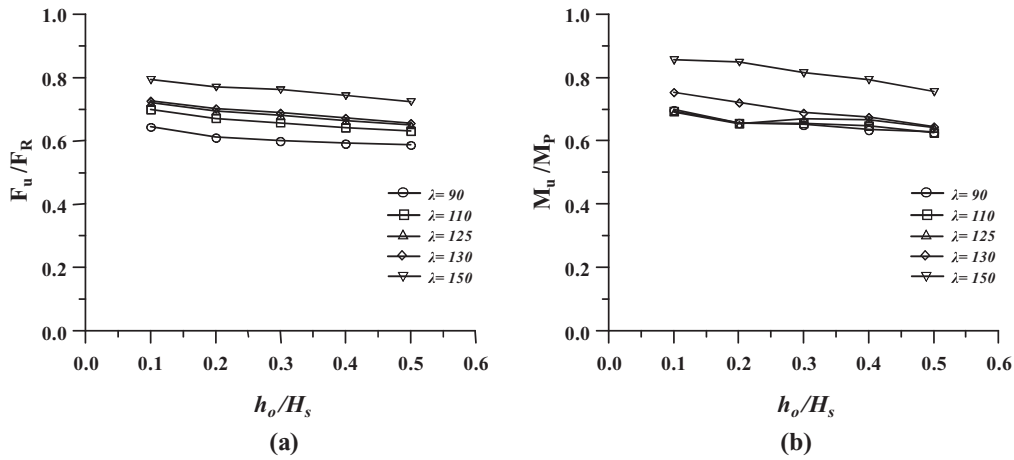


Figure 20. Summary of non-dimensionalised load-carrying capacity with varying cutout's location in the vertical direction: (a) axial compression; (b) pure bending.

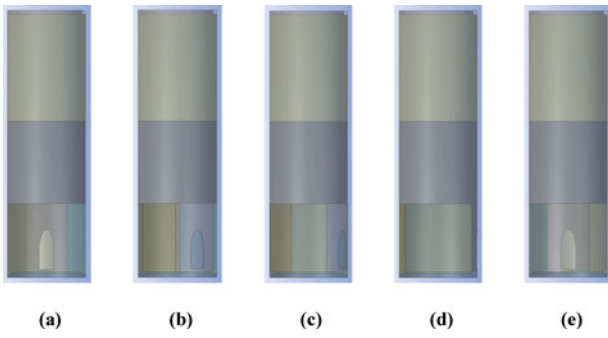


Figure 21. An example of applied geometries varying cutout's angle in circumferential direction: (a)  $\theta = 0^\circ$ ; (b)  $\theta = 30^\circ$ ; (c)  $\theta = 60^\circ$ ; (d)  $\theta = 90^\circ$ ; (e)  $\theta = 180^\circ$ . (This figure is available in colour online.)

column slenderness ratio decreases, the reduction rate increases under both loading conditions. Moreover, the ultimate strength under pure bending is not sensitive to the variations in the column slenderness ratio; namely, increasing diameter except for  $\lambda = 150$ .

### 5.2.2. Circumferential direction

The thickness,  $t$ , is kept the same at 30 mm under pure bending to identify the effects that cutout location in the circumferential direction has on the ultimate strength because the structural response under axial compression is symmetrical. Ninety cases of series analyses are performed in total, and the parameters considered are as follows:

- Shape: half-rectangular-elliptical
- Column slenderness ratio,  $\lambda = D/t$ : 125
- Cutout angle,  $\theta$ :  $0^\circ, 15^\circ, 30^\circ, 45^\circ, 60^\circ, 90^\circ, 120^\circ, 150^\circ, 180^\circ$
- Loading condition: pure bending

Figure 21 illustrates an example of applied geometries with varying cutout angles in the circumferential direction,  $\theta = 0^\circ - 180^\circ$ .

Figure 22 presents an example of moment-rotation histories with varying cutout angles and the non-dimensionalised load-carrying strength. It confirms that when a cutout is located on

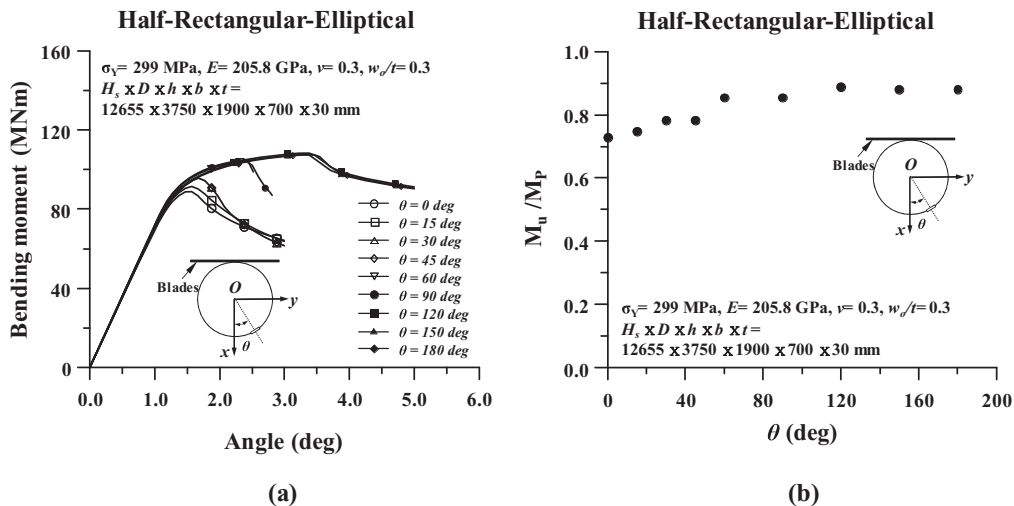


Figure 22. Effect of cutout's angle under pure bending: (a) moment-rotation histories; (b) non-dimensionalised load-carrying strength.

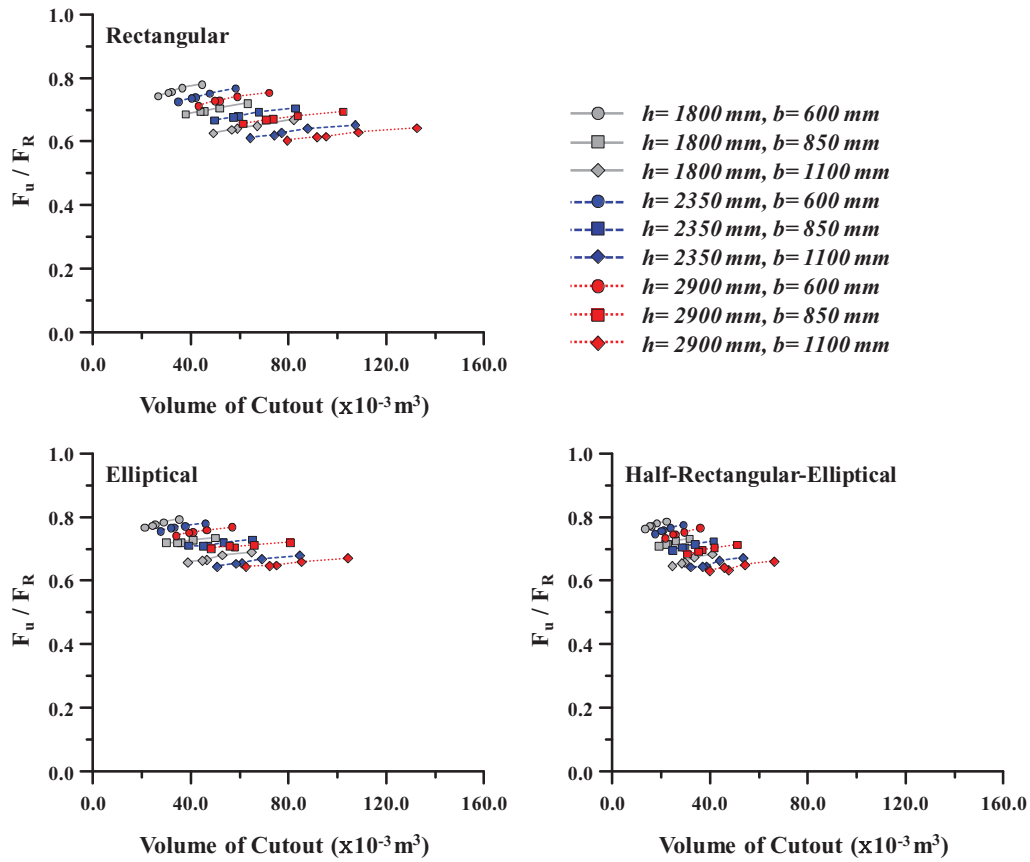


Figure 23. An example of the effect of column slenderness ratio for  $D = 3,750 \text{ mm}$  under axial compression. (This figure is available in colour online.)

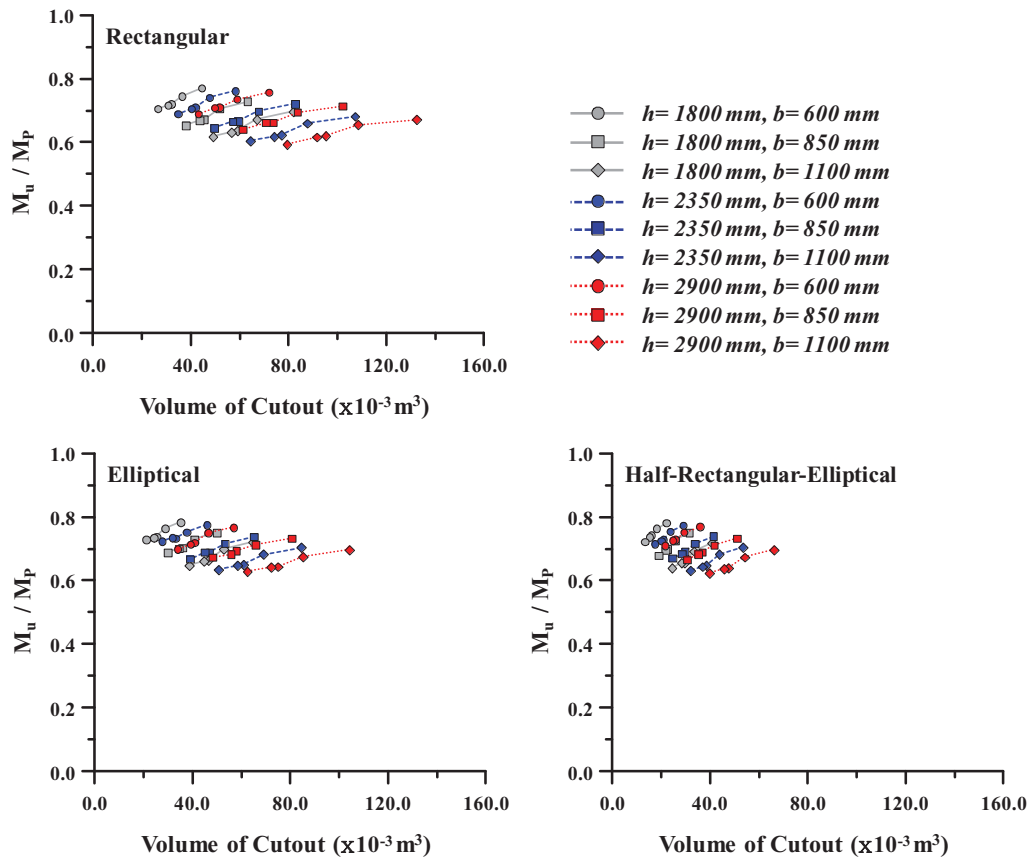


Figure 24. An example of the effect of column slenderness ratio for  $D = 3,750 \text{ mm}$  under pure bending. (This figure is available in colour online.)

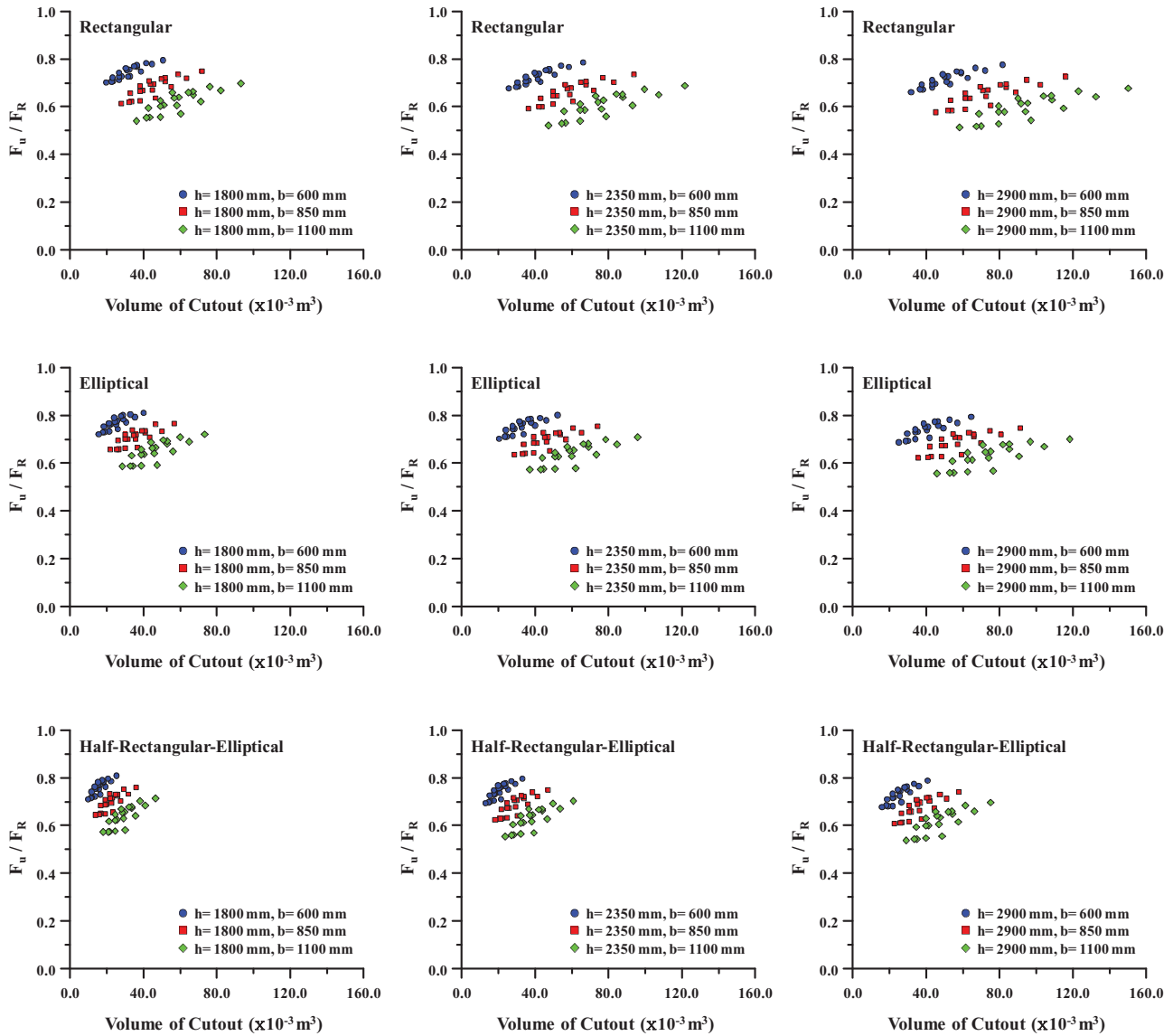


Figure 25. Summary of the non-dimensionalised ultimate strength under axial compression. (This figure is available in colour online.)

the compression side ( $\theta = 0^\circ$ ), the ultimate strength is minimal, and as the cutout angle increases, so do the ultimate strength. It is observed that the ultimate strength increases almost linearly until  $\theta = 90^\circ$ , whereas it appears almost constant over  $90^\circ$  ( $\theta = 120^\circ, 150^\circ, 180^\circ$ ).

### 5.3. Combined effects of aspect, column slenderness and column aspect ratios

To examine the effects of the aspect, column slenderness and column aspect ratios on the ultimate strength, the dimensions of the cutouts vary based on the statistical distribution boundaries,  $1800 \leq h \leq 2900$  and  $600 \leq b \leq 1100$ , as illustrated in Section 3.2. For the selection of parameters, DOE is applied, using the CCD method. Four cases of the maximum diameter varying from 2750 to 4250 mm are noted with the locations of the cutouts in the vertical and circumferential directions,  $h_o/H_S = 0.1$  and  $\theta = 0^\circ$ . A total of 1080 cases of series analyses are performed, and the parameters considered are as follows:

- Shape: rectangular, elliptical, half-rectangular-elliptical
- Height of the cutout,  $h$ : 1800–2900 mm
- Width of the cutout,  $b$ : 600–1100 mm
- Diameter,  $D$ : 2750, 3250, 3750, 4250 mm
- Column slenderness ratio,  $\lambda = D/t$ : 90, 110, 125, 130, 150
- Loading condition: axial compression and pure bending

The volume of the cutout is defined as

$$V = At \quad (3)$$

where  $V$  is the volume of the cutout,  $A$  is its area and  $t$  is the thickness of the wind turbine tower. It is assumed that the change in the breadth of the cutout due to curvature is ignored to simplify the calculation of the cutout area.

Figures 23 and 24 show an example of the effect of column slenderness and aspect ratios on the non-dimensionalised ultimate strength ( $D = 3750$  mm) for three shapes under axial compression and pure bending. It is found that as the height

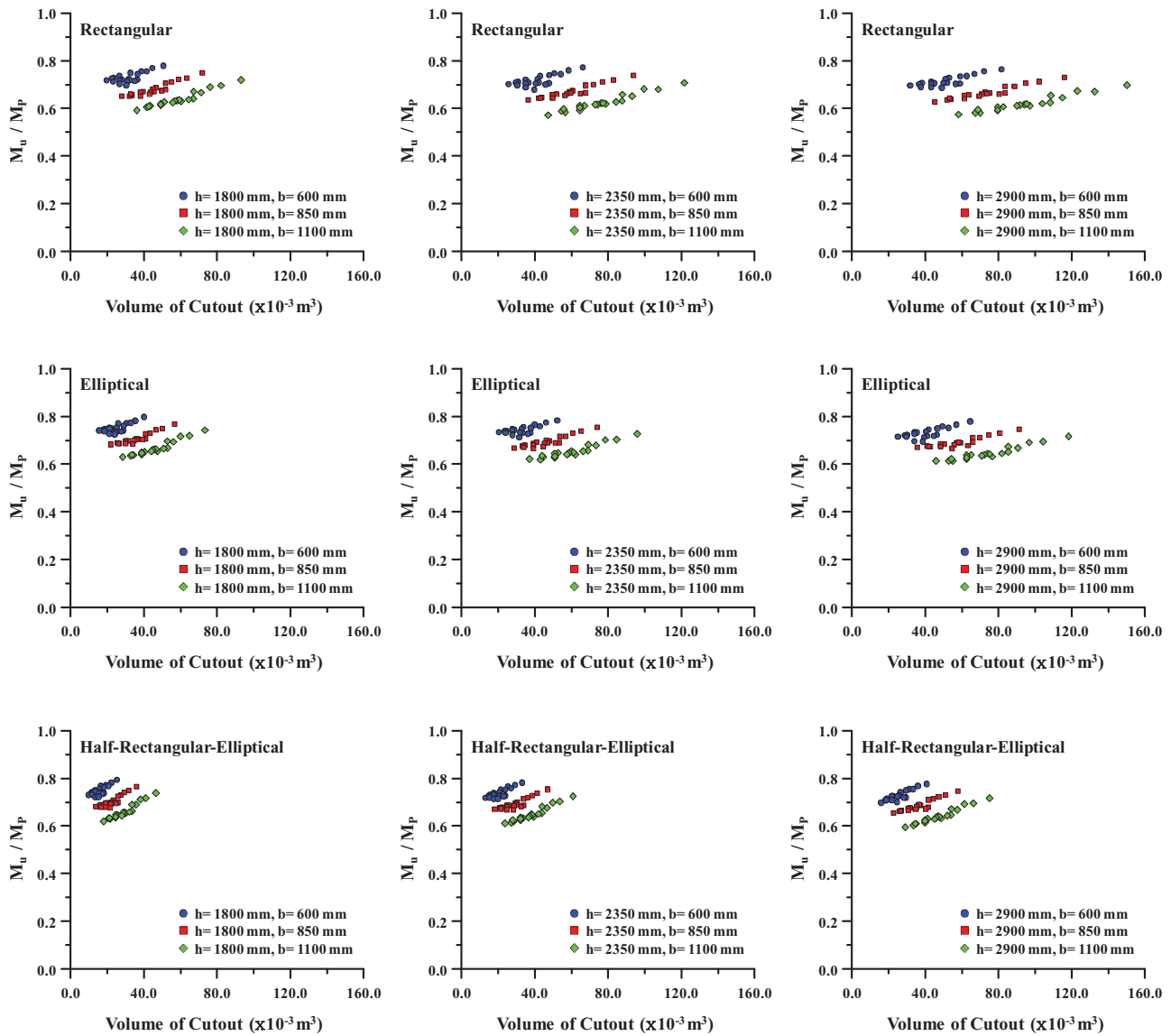


Figure 26. Summary of the non-dimensionalised ultimate strength under pure bending. (This figure is available in colour online.)

of the cutout,  $h$  increases for the same breadth,  $b$ , the ultimate strength clearly decreases. It is observed that as the volume of the cutout increases for the same aspect ratio, the strength decreases due to increasing thickness, yet the reduced ultimate strength appears nearly the same regardless of the cutout shape.

Figures 25 and 26 illustrate the non-dimensionalised ultimate strength of selected design points for the three cutout shapes under axial compression and pure bending. It is found that the ultimate-strength reduction appears within a range of 50%–80% of the reference strengths for both loading conditions.

## 6. Empirical formulation of the ultimate strength

The results of the parametric analysis described in Section 5.3 are used to derive empirical formulations that can predict the ultimate strength of a circular cylindrical shell with the cutout. The linear regression approach with the least-squares method is used as follows:

$$F_u/F_R = \xi_D D + \xi_t t + \xi_h h + \xi_b b + \xi_C \quad (4)$$

$$M_u/M_P = \zeta_D D + \zeta_t t + \zeta_h h + \zeta_b b + \zeta_C \quad (5)$$

where  $F_u/F_R$  and  $M_u/M_P$  are the non-dimensionalised ultimate strengths under axial compression and pure bending, respectively. The coefficients for axial compression and pure bending are indicated in Table 4. The regression statistics, including the correlation coefficients and the adjusted  $R$ -square ( $R^2$ ), are illustrated in Table 5.

The correlation between the numerical results and the empirical estimations of the ultimate strength is illustrated in Figure 27. It is found that the estimations made by the proposed empirical equations well agree with the numerical calculations. This implies that the proposed empirical equations can be an effective way to estimate the reduced ultimate strength of circular cylindrical shells with cutouts.

Empirical formulae developed in the present study cover an extensive range of possible geometrical variations in circular

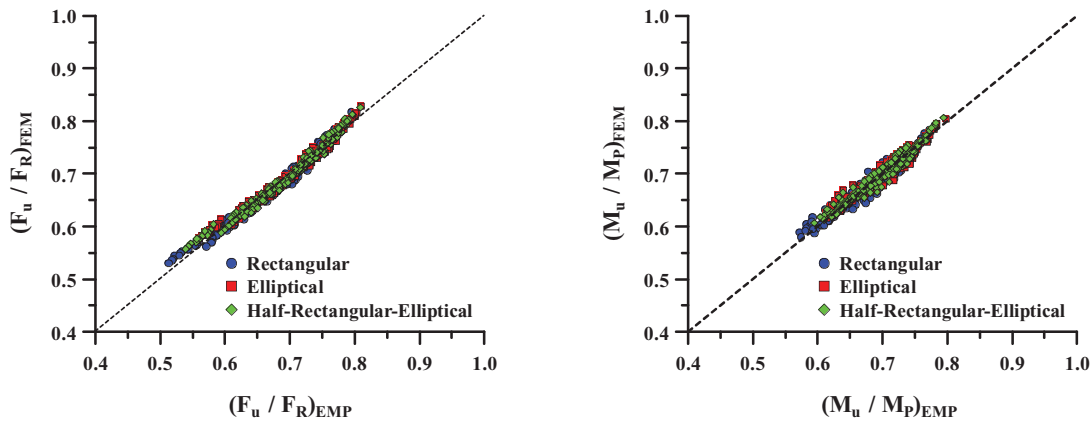


Figure 27. Correlation between the FEA and empirical estimation on the ultimate strength. (This figure is available in colour online.)

Table 4. Coefficients of design formula.

Shape	Axial compression				
	$\xi_D (10^{-4})$	$\xi_t (10^{-3})$	$\xi_h (10^{-4})$	$\xi_b (10^{-3})$	$\xi_C$
Rectangular	0.499	1.998	-0.246	-0.243	0.692
Elliptical	0.518	1.198	-0.212	-0.227	0.717
Half-rectangular-elliptical	0.524	1.491	-0.236	-0.233	0.707
Shape	Pure bending				
	$\zeta_D (10^{-4})$	$\zeta_t (10^{-3})$	$\zeta_h (10^{-4})$	$\zeta_b (10^{-3})$	$\zeta_C$
Rectangular	-0.141	4.250	-0.151	-0.187	0.791
Elliptical	-0.144	3.661	-0.175	-0.172	0.827
Half-rectangular-elliptical	-0.148	3.984	-0.175	-0.176	0.818

Table 5. Regression statistics.

Shape	Axial compression		Pure bending	
	$\sigma$	$R^2$	$\sigma$	$R^2$
Rectangular	0.989	0.978	0.975	0.950
Elliptical	0.989	0.977	0.972	0.943
Half-rectangular-elliptical	0.989	0.978	0.978	0.956

cylindrical shells with cutouts, and thus they would provide guidance for wind turbine tower design. It should be cautioned that they may need to be validated further by comparison with more accurate computations and experiments before being used in special cases with geometric and boundary conditions.

## 7. Conclusion

The aims of this study are to develop a numerical modelling technique that accurately predicts structural responses by considering nonlinearities, and to numerically examine the effects of various variables on the ultimate-strength characteristics of wind turbine towers with cutouts. A series of nonlinear finite element computations were undertaken to achieve these objectives, and several conclusions can be drawn from the results, as outlined below.

- (1) First, the wind turbine structures in service were investigated, and their actual dimensional characteristics and those of their cutouts were identified from the data collected and analysed.

- (2) A nonlinear finite-element modelling technique was developed based on a mesh-convergence study and validation studies for wind turbine towers with cutouts.
- (3) It was confirmed that the effect of the cutout shape is negligible, whereas placing the cutout on the compression side produced the minimum ultimate strength.
- (4) Although the closest cutout near the fixed boundary revealed the highest ultimate strength for axial compression and pure bending, it cannot be regarded as the safest wind turbine in terms of structural integrity due to a sudden drop in strength was measured after the ultimate state. Further, under pure bending, the ultimate strength appeared to be uniform when the cutout angle was over 90°.
- (5) Based on the results of a parametric analysis, an empirical formula accommodating a whole range of actual dimensional characteristics is proposed only for axial compression and pure bending. This formula has the potential to improve the design and safety assessment of circular cylindrical shells with cutouts.
- (6) Given the numerous uncertainties involved due to geometrical and boundary conditions, among others, further studies are recommended to examine models used to examine the collapse mechanism more realistically.


## Disclosure statement

No potential conflict of interest was reported by the authors.

## Funding

This research was supported by Basic Science Research Program through the National Research Foundation of Korea (NRF) funded by the Ministry of Education [grant number NRF-2014R1A1A2006102], [grant number NRF-2015R1A6A3A01060166]; Leading Foreign Research Institute Recruitment Program through the National Research Foundation of Korea (NRF) funded by the Ministry of Science, Ict & future Planning(MSIP) [grant number 2013044761].

## ORCID

Sang Eui Lee  <http://orcid.org/0000-0002-6952-9071>

## References

- ANSYS. 2015. User's manual (version 16.1). Canonsburg (PA): ANSYS Inc.
- Azizian ZG, Roberts TM. 1983. Buckling and elasto-plastic collapse of perforated plates. In: Morris LJ, editor. Proceedings of the international

- conference on instability and plastic collapse of steel structures. London: Granada Publishing; p. 392–398.
- Betten J, Shin CH. 2000. Elasto-plastic buckling analysis of rectangular plates subjected to biaxial loads. *Forsch Ingenieurwes.* 65:273–278.
- Brazier LG. 1927. On the flexure of thin cylindrical shells and other “thin” sections. *Proc R Soc Lond A.* 116: 104–114. doi:10.1098/rspa.1927.0125
- Brown CJ, Yettam AL. 1986. The elastic stability of square perforated plates under combinations of bending, shear and direct load. *Thin-Walled Struct.* 4: 239–246.
- Dimopoulos CA, Gantes CJ. 2012. Experimental investigation of buckling of wind turbine tower cylindrical shells with opening and stiffening under bending. *Thin-Walled Struct.* 54:140–155.
- Dimopoulos CA, Gantes CJ. 2013. Comparison of stiffening types of the cutout in tubular wind turbine towers. *Jurnal of Constructional Steel research.* 83:62–74.
- Dimopoulos CA, Gantes CJ. 2015. Numerical methods for the design of cylindrical steel shells with unreinforced or reinforced cutouts. *Thin-Walled Structures.* 96:11–28.
- Dimopoulos CA, Koulatzou K, Petrini F, Gantes CJ. 2015. Assessment of stiffening type of the cutout in tubular wind turbine towers under artificial dynamic wind actions. *Journal of computational and nonlinear dynamics.* 10. doi: <http://dx.doi.org/10.1115/1.4028074>
- DIN 18800-4. 1990. *Stahlbauten: Stabilitätsfälle, Schalenbeulen* [Steel structure-Part 4: Stability - Safety against buckling of shells, German Institute for Standardization]. Berlin: Beuth Verlag.
- DNVGL. 2013a. Design of offshore wind turbine structures, Report No.: DNV-OS-J101. Oslo (Norway): Det Norske Veritas
- DNVGL. 2013b. Buckling strength of shells, DNV-RP-C202. Oslo: Det Norske Veritas.
- Durban D, Zuckerman Z. 1999. Elasto-plastic buckling of rectangular plates in biaxial compression/tension. *Int J Mech Sci.* 41: 751–765.
- [ECCS] European Convention for Constructional Steelwork. 1980. Technical committee 8, structural stability, TWG 8.4- Shells, buckling of steel shells. 1st ed. *European Design Recommendations.*
- El-Sawy KM, Nazmy AS, Martini MI. 2004. Elasto-plastic buckling of perforated plates under uniaxial compression. *Thin-Walled Struct.* 42:1083–1101.
- EN1993-1.6. 2006. European committee for standardization, Eurocode 3: design of steel structures, Part 1–6. *Strength Stability Shell Struct.*
- Fabian O. 1977. Collapse of cylindrical, elastic tubes under combined bending, pressure and axial loads. *Int J Solids Struct.* 13: 1257–1270.
- Gellin S. 1980. The plastic buckling of long cylindrical shell under pure bending. *Int J Solids Struct.* 16: 397–407.
- Ghanbari Ghazijahani T, Jiao H, Holloway D. 2015. Structural behaviour of shells with different cutouts under compression: an experimental study. *J Const Steel Res.* 105: 129–137.
- Guo L, Yang S, Jiao H. 2013. Behaviour of thin-walled circular hollow section tubes subjected to bending. *Thin-Walled Struct.* 73: 281–289.
- Han H, Cheng J, Taheri F, Pegg N. 2006. Numerical and experimental investigations of the response of aluminum cylinders with a cutout subject to axial compression. *Thin-Walled Struct.* 44: 254–270.
- Ju GT, Kyriakides S. 1992. Bifurcation and localization instabilities in cylindrical shells under bending II. Predictions. *Int J Solids Struct.* 29: 1143–1171.
- Jullien J, Limam A. 1998. Effects of openings of the buckling of cylindrical shells subjected to axial compression. *Thin-Walled Struct.* 31: 187–202.
- Kim UN, Choe IH, Paik JK. 2009. Buckling and ultimate strength of perforated plate panels subject to axial compression: experimental and numerical investigations with design formulations. *Ships Offshore Struct.* 4: 337–361.
- Kyriakides S, Ju GT. 1992. Bifurcation and localization instabilities in cylindrical shells under bending. I. Experiments. *Int J Solids Struct.* 29:1117–1142.
- Lee SE, Paik JK, Ha YC, Kim BJ, Seo JK. 2014. An efficient design methodology for subsea manifold piping systems based on parametric studies. *Ocean Eng.* 84: 273–282.
- Paik JK. 2007. Ultimate strength of steel plates with a single circular hole under axial compressive loading along short edges. *Ships Offshore Struct.* 2:355–360.
- Reissner E. 1961. On finite pure bending of cylindrical tubes. *Österreichisches Ingenieur-Archiv.* 15: 165–172.
- Sabir AB, Chow FY. 1983. Elastic buckling of flat panels containing circular and square holes. In: *Proceedings of the International Conference on Instability and Plastic Collapse of Steel Structures.* London, UK: Granada Publishing; p. 311–321.
- Sahin S. 2016. Wind turbine tower structures analysis according to wind load in terms of cost [thesis]. Szczecin: University of Liege.
- Schenk CA, Schuëller GI. 2007. Buckling analysis of cylindrical shells with cutouts including random boundary and geometric imperfections. *Comput Method Appl Mech Eng.* 196:3424–3434.
- Seide P, Weingarten VI. 1961. On the buckling of circular cylindrical shells under pure bending. *J Appl Mech.* 28: 112–116.
- Shangmugam NE, Thevendran V, Tan YH. 1999. Design formula for axially compressed perforated plates. *Thin-Walled Struct.* 34: 1–20.
- Shariati M, Rokhi MM. 2008. Numerical and experimental investigations on buckling of steel cylindrical shells with elliptical cutout subject to axial compression. *Thin-Walled Struct.*, 46:1251–1261.
- Shariati M, Rokhi MM. 2010. Buckling of steel cylindrical shells with an elliptical cutout. *Int J Steel Struct.* 10:193–205.
- Sherman DR. 1976. Tests of circular steel tubes in bending. *ASCE J Struct Div.* 102:2181–2195.
- Tennyson RC. 1968. The effects of unreinforced circular cutouts on the buckling of circular cylindrical shells under axial compression. *J Eng Ind.* 90:541–546.
- Wang G, Sun H, Peng H, Uemori R. 2009. Buckling and ultimate strength of plates with openings. *Ships Offshore Struct.* 4:43–53.
- Yeh MK, Lin MC, Wu WT. 1999. Bending buckling of an elasto-plastic cylindrical shell with a cutout. *Eng Struct.* 21: 996–1005.



## Appendix

Table A1. Principal dimensions of wind turbines and cutouts.

No.	Capacity (MW)	$H$ (mm)	$D_{\min}$ (mm)	$D_{\max}$ (mm)	$t_{\min}$ (mm)	$t_{\max}$ (mm)	$h$ (mm)	$b$ (mm)	$t$ (mm)
1	1.0	45,000	2090	3280	10	18	2000	700	18
2	2.0	50,000	2560	4150	16	36	2550	850	36
3	2.0	53,000	2580	4040	18	36	2550	850	36
4	3.0	65,000	2280	4150	14	28	2550	850	28
5	3.0	60,000	2350	4052	16	32	2550	850	32
6	5.0	75,000	2450	6000	16	27	2550	850	27
7	5.0	75,000	2570	6000	16	27	2550	850	27
8	0.45	37,000	1820	2800	10	16	2050	700	16
9	0.6	40,000	1800	2720	10	18	2180	720	18
10	2.0	60,000	2300	3750	18	30	2690	1100	30
11	3.0	100,000	2540	4500	18	30	2150	703	30
12	4.0	92,000	2460	4300	14	30	2540	990	30
13	3.5	88,000	2320	4150	16	34	1640	750	34
14	2.0	76,000	3000	4300	12	30	2150	850	30
15	3.7	77,000	3000	4000	15	40	2900	850	40
16	2.0	50,000	2850	4150	20	40	2900	850	40
17	3.0	65,000	2294	3650	14	28	1997	750	28
18	3.2	60,000	2150	3720	16	32	2080	800	32
19	2.0	48,000	2000	3570	18	34	1850	680	34
20	4.2	88,000	2380	4420	14	34	2200	850	34
21	2.6	70,000	2210	2980	16	28	1920	700	28
22	2.2	65,000	2370	3020	16	28	1900	680	28
23	2.7	69,000	2450	2950	14	30	2100	680	30
24	3.4	70,000	2340	3800	16	30	2020	750	30
25	4.2	80,000	2240	3650	14	32	1980	680	32
26	2.0	55,000	2200	3400	14	28	1900	720	28
27	2.9	85,000	2320	3860	14	30	2080	780	30
28	2.9	75,000	2460	3680	14	28	2280	820	28
29	1.8	50,000	1780	2900	16	28	1870	690	28
30	3.7	78,000	2240	3780	14	32	1990	750	32
31	3.0	70,000	2370	3720	14	28	1930	680	28
32	1.8	55,000	1890	2890	16	28	1880	680	28
33	2.2	60,000	1920	3220	14	30	2050	720	30
34	3.4	78,000	2360	3680	14	30	1990	680	30

**Table A2.** Principal dimensions of wind turbines and cutouts.

No.	Capacity (MW)	H (mm)	$D_{\min}$ (mm)	$D_{\max}$ (mm)	$t_{\min}$ (mm)	$t_{\max}$ (mm)	h (mm)	b (mm)	t (mm)
35	3.2	65,000	2280	3540	16	28	1920	800	28
36	2.6	55,000	2360	3640	14	26	1900	680	26
37	1.8	50,000	1760	2700	14	28	1840	680	28
38	1.7	55,000	1680	2740	12	26	1900	650	26
39	3.5	68,000	2320	3640	14	30	1960	700	30
40	2.7	65,000	2240	3580	14	32	1990	780	32
41	3.4	84,000	2450	3840	16	28	2000	800	28
42	3.0	65,000	2280	3480	16	30	1980	720	30
43	1.6	50,000	1780	2690	14	28	1780	780	28
44	2.6	60,000	1880	3640	16	30	1990	680	30
45	3.0	70,000	2264	3700	12	32	2040	720	32
46	3.6	68,000	2380	3680	14	32	1980	640	32
47	2.3	50,000	2210	3200	12	28	1880	684	28
48	1.8	50,000	1760	2700	14	28	1840	680	28
49	1.6	55,000	1720	2860	12	28	1880	650	28
50	3.6	73,000	2260	3680	14	32	1994	686	32
51	2.4	55,000	2200	3400	14	28	1800	640	28
52	4.1	78,000	2260	4100	14	32	2100	780	32
53	1.8	52,000	2140	3360	12	22	1980	720	22
54	2.6	65,000	2420	3860	16	32	2860	780	32
55	2.4	60,000	2380	3900	16	34	2200	650	34
56	2.0	55,000	1980	3450	12	30	2640	700	30
57	3.4	65,000	2340	3640	14	34	1980	660	34
58	1.9	50,000	1840	2640	14	26	2000	700	26
59	5.0	88,000	2570	4230	16	32	2240	650	32
60	0.8	40,000	1750	2900	10	28	1990	650	28
61	4.0	80,000	1900	2890	14	28	2000	720	28
62	2.0	64,000	2320	3840	14	30	2720	980	30
63	3.2	80,000	2640	3840	14	32	2080	680	32
64	4.0	75,000	2360	4180	14	28	2120	640	28
65	3.1	65,000	2240	3680	16	32	1970	680	32
66	4.0	80,000	2320	3860	12	28	1990	690	28
67	3.4	83,000	2360	3940	12	32	2220	710	32
68	2.4	60,000	2240	2940	10	28	1940	650	28

**Table A3.** Principal dimensions of wind turbines and cutouts.

No.	Capacity (MW)	H (mm)	$D_{\min}$ (mm)	$D_{\max}$ (mm)	$t_{\min}$ (mm)	$t_{\max}$ (mm)	h (mm)	b (mm)	t (mm)
69	1.8	50,000	1780	2680	12	24	1890	640	24
70	2.1	74,000	2400	3620	10	32	2100	680	32
71	3.4	78,000	2180	3680	12	34	2200	740	34
72	2.2	52,000	1860	2870	10	28	2050	650	28
73	2.8	68,000	2150	3720	12	32	1940	680	32
74	3.4	68,000	2240	3640	14	28	2000	660	28
75	2.2	55,000	1990	2870	16	30	1980	720	30
76	3.9	84,000	2280	3640	14	28	2120	750	28
77	2.6	80,000	2180	3640	12	30	1990	680	30
78	2.4	60,000	2120	3360	12	32	1970	710	32
79	2.6	67,000	2240	3420	12	26	1990	672	26
80	3.1	80,000	2180	3640	14	32	1940	690	32
81	3.0	72,000	2140	3480	12	32	2130	700	32
82	2.1	65,000	1960	3580	12	32	1980	640	32
83	3.3	80,000	2240	4000	12	32	2200	840	32
84	2.4	64,000	2260	3800	14	32	2120	680	32
85	1.7	52,000	1790	3140	12	32	1980	720	32
86	3.7	78,000	2240	3780	14	32	1990	750	32
87	2.8	72,000	2260	3450	12	30	2050	750	30
88	1.9	55,000	1680	3120	12	30	1960	724	30
89	2.4	68,000	1890	3480	13	28	2150	750	28
90	3.7	87,000	2480	3780	12	32	2040	750	32
91	3.4	80,000	2340	3750	14	32	2000	810	32
92	2.7	68,000	2180	3580	12	30	2000	780	30
93	2.1	64,000	1860	2940	10	28	1960	680	28
94	2.0	60,000	1600	2900	16	30	1880	750	30
95	3.2	66,000	2200	3690	10	28	1890	690	28
96	2.4	60,000	2140	3640	10	30	1800	640	30
97	3.0	80,000	2200	3450	12	30	1920	740	30
98	2.4	72,000	2180	3590	14	32	2100	720	32
99	1.4	45,000	1640	2610	10	26	1680	620	26
100	3.1	65,000	1960	3580	12	28	1890	690	28
101	2.7	65,000	2230	3690	14	28	2200	740	28
102	3.4	73,000	2240	3640	12	27	2050	700	27